Mafic dykes of the southeastern Gawler Craton: *ca* 1564 Ma magmatism with an enriched mantle source

A. J. Reid, C. E. Wade & E. A. Jagodzinski

View supplementary material

Published online: 20 Jan 2022.

Submit your article to this journal

Article views: 712

View related articles

View Crossmark data

Mafic dykes of the southeastern Gawler Craton: *ca* 1564 Ma magmatism with an enriched mantle source

A. J. Reid[a,b] 🆔, C. E. Wade[a] 🆔 and E. A. Jagodzinski[a] 🆔

[a]Geological Survey of South Australia, Department for Energy and Mining, Adelaide, Australia; [b]Department of Earth Sciences, University of Adelaide, Adelaide, Australia

ABSTRACT

This study investigates the age and composition of a suite of mafic dykes in the southeastern Gawler Craton. Mafic dykes intrude the gneissic fabric of the *ca* 1850 Ma Donington Suite and were previously interpreted to have been emplaced at *ca* 1845 Ma. However, sensitive high-resolution ion microprobe U–Pb dating of zircon within one of these mafic dykes shows it was emplaced at 1564 ± 4 Ma. The sampled dyke also contains a population of inherited zircon cores with an age of 1770 ± 6 Ma, and one grain with an age of *ca* 1860 Ma, likely derived from country rock. Whole-rock geochemistry from this dyke and nearby dykes with similar structural and mineralogical features show that there is a suite of dykes in the region with gabbroic, low SiO_2 and TiO_2 contents and tholeiitic characteristics. The dykes are enriched in Ba, K and Rb, with low to moderate MgO, Ni and Cr contents, and moderate light rare earth element enrichment. Negative Nb and Ta anomalies with subtle negative Ti anomalies suggest some interaction with continental crust. Sm–Nd isotopic data have $\varepsilon_{Nd(1560\,Ma)}$ between -6.8 and -2.9, and depleted mantle model ages >2.5 Ga. Th/Nb ratios are 0.21–0.73 consistent with a metasomatised, subduction modified lithospheric mantle source. The relatively primitive nature of the tholeiites suggests the crustal-like signatures are inherited from the source region, which likely represents an enriched continental lithospheric mantle in the eastern Gawler Craton. This *ca* 1564 Ma mafic magmatism is newly named the Daly Head Metadolerite. In addition, narrow high-strain zones overprint the dated mafic dyke and locally the Donington Suite wall rocks. A syn-kinematic granitic dyke intrusion within one high-strain zone has been dated via laser ablation-inductively coupled plasma mass spectrometry U–Pb zircon methods and was emplaced at *ca* 1555 Ma. This localised *ca* 1555 Ma deformation is a previously unrecognised tectonic event in the southern Gawler Craton. This study adds to the growing database showing magmatism and deformation in the Gawler Craton continued after the voluminous Gawler Range Volcanics and Hiltaba Suite magmatism (*ca* 1596–1575 Ma). These younger tectono-magmatic events typically occur around the margins of the Gawler Craton, suggesting the internal 'core' of the craton may have been substantially less fertile for melting during these younger thermal/structural events, likely because of the high-temperature nature of the early Mesoproterozoic Gawler Range Volcanics and Hiltaba Suite magmatism.

KEY POINTS

1. Geochronology shows mafic dykes in southeastern Gawler Craton emplaced at 1564 ± 4 Ma.
2. Mafic dykes are tholeiitic, derived from a metasomatised, subduction modified lithospheric mantle source.
3. Narrow high-strain zones overprint the dated mafic dyke and contain syn-kinematic granitic dyke dated at *ca* 1555 Ma.
4. Localisation of post-*ca* 1575 Ma tectono-magmatic events occur around margins of the craton, reflecting reduced melt fertility in the centre owing to previous high-temperature events.

Introduction

Our understanding of the tectonic evolution of the Gawler Craton, South Australia, has undergone significant changes in the past two decades (*e.g.* Daly *et al.*, 1998; Hand *et al.*, 2007; Parker *et al.*, 1993; Skirrow *et al.*, 2018). However, the majority of recent studies have focused on felsic magmatic rocks or metasedimentary units (*e.g.*, Howard *et al.*, 2011; Payne *et al.*, 2006; Reid & Payne, 2017). There have been relatively few studies that have looked at the mafic rocks of the Gawler Craton in order to investigate the

mantle–crust interaction through time (*e.g.* Huang *et al.*, 2015, 2016; Skirrow *et al.*, 2018; Wade *et al.*, 2019).

The majority of studies of magmatism in the Gawler Craton have focused on the widespread and metallogenically significant event that occurred in the early Mesoproterozoic, *ca* 1595–1575 Ma. During this time period, extensive bimodal magmatism of the Hiltaba Suite and Gawler Range Volcanics formed, along with a range of ore deposits, including Olympic Dam, Prominent Hill and Carrapateena of the iron oxide–copper–gold class (*e.g.* Allen *et al.*, 2008; Budd, 2006; Courtney-Davies *et al.*, 2020; Ehrig *et al.*, 2012; Reid, 2019; Wade *et al.*, 2019). There is, however, a small but growing body of evidence that there are younger magmatic events preserved in the Gawler Craton, for example, *ca* 1555–1530 Ma granite in the northeast Gawler Craton (Peak and Denison inliers; Fanning *et al.*, 2007), *ca* 1515 Ma granite in the Mt Woods region (Jagodzinski & Reid, 2015), *ca* 1500 Ma granites in the southeast Gawler Craton (Spilsby Suite; Fanning *et al.*, 2007; Rankin *et al.*, 2006; Reid *et al.*, 2020) and *ca* 1450 to *ca* 1380 Ma granites in the northern Gawler Craton (Morrissey *et al.*, 2019; Reid & Forster, 2021). The tectonic drivers for these magmatic events are poorly understood, and more data are needed to build up the regional picture of the extent of this magmatism. These younger magmatic events may in turn be significant for understanding larger scale tectonic systems, as these are magmatic events that occurred around the time of breakup of the supercontinent Nuna (Aitken *et al.*, 2016; Betts *et al.*, 2016; Giles *et al.*, 2004; Morrissey *et al.*, 2019; Reid & Forster, 2021; Tiddy & Giles, 2020).

In the southeastern Gawler Craton, South Australia, coastal exposures of the Southern Yorke Peninsula reveal a series of mafic dykes that intrude Paleoproterozoic granite and gneiss. These mafic dykes have been interpreted to have formed during late orogenic extension during the Paleoproterozoic (*e.g.* Reid *et al.*, 2008; Zang, 2006). However, no geochronological evidence has previously been available with which to assess the age of mafic dyke intrusion. In this contribution, we present zircon U–Pb geochronology, whole-rock geochemistry and Sm–Nd isotopic data for these dykes that show they were emplaced during the Mesoproterozoic. The new data reveal the presence of a new mafic dyke unit, the Daly Head Metadolerite (new name). The Daly Head Metadolerite is part of a spatially distributed series of magmatic and/or deformation events that have been documented from regions external to the central 'core' of the Gawler Craton and post-date the well-known and economically significant Gawler Range Volcanics–Hiltaba Suite magmatism.

Geological setting

The Gawler Craton is built predominantly on Mesoarchean and Neoarchean to earliest Paleoproterozoic basement (Fraser *et al.*, 2010; Reid *et al.*, 2014) and the meta-igneous and metasedimentary geological units of the Gawler Craton are mostly Paleoproterozoic in age (Figures 1–3). These Paleoproterozoic units include the *ca* 1850 Ma Donington Suite, which occurs in the eastern Gawler Craton, and is granitic to charnockitic in composition and associated with co-magmatic mafic rocks of the Jussieu Metadolerite (Mortimer *et al.*, 1988; Parker *et al.*, 1993; Reid *et al.*, 2008; Schwarz, 2003; Zang, 2006). The Donington Suite is interpreted to have formed from melting of a primitive mantle source substantially contaminated by Archean lower crust (Hoek & Schaefer, 1998; Schaefer, 1998). The Donington Suite was associated with a phase of localised high-temperature–medium-pressure metamorphism and deformation known as the Cornian Orogeny (Reid *et al.*, 2008). In the eastern Gawler Craton, the Donington Suite is overlain by a *ca* 1765–1735 Ma metasedimentary and metavolcanic succession, known as the Wallaroo Group (Cowley *et al.*, 2003; Fanning *et al.*, 2007). The Wallaroo Group is one of a series of Paleoproterozoic cover units that occur across the Gawler Craton, such as the Hutchison Group in the south and metasedimentary units of the Nawa Domain in the north (Hand *et al.*, 2007).

Widespread high-temperature metamorphism, deformation and syn- and post-orogenic magmatism affected large regions of the Archean basement and Paleoproterozoic cover sequences during the *ca* 1735–1690 Ma Kimban Orogeny (*e.g.* Hand *et al.*, 2007). Subsequent to this, the geological record in the Gawler Craton is dominated by magmatism. Significant magmatic suites include the *ca* 1690–1670 Ma Tunkillia Suite (Payne *et al.*, 2010), the *ca* 1635–1605 Ma St Peter Suite (Flint *et al.*, 1990; Reid *et al.*, 2020), and the voluminous *ca* 1595–1575 Ma Hiltaba Suite and Gawler Range Volcanics (Blissett *et al.*, 1993; Flint *et al.*, 1993). Mafic and felsic magmatism of this age is abundant in north-central Yorke Peninsula (Conor, 1995; Zang *et al.*, 2007).

The Gawler Craton was deformed and variably metamorphosed during and subsequent to the Hiltaba Suite and Gawler Range Volcanics magmatic event, in the Kararan Orogeny (Brotodewo *et al.*, 2018; Conor *et al.*, 2010; Hand *et al.*, 2007; Skirrow *et al.*, 2018; Tiddy *et al.*, 2020; Tiddy & Giles, 2020). This magmatic-tectonic event was associated with mineralisation across the Gawler Craton (Budd & Fraser, 2004; Reid, 2019; Skirrow *et al.*, 2007), including Cu–Au mineralisation on the Yorke Peninsula (*e.g.* Moonta-Wallaroo and Hillside deposits; Conor *et al.*, 2010).

The Gawler Craton was variably reworked over the interval *ca* 1565 Ma through to *ca* 1450 Ma with deformation and magmatic events occurring across the northern, western and southeastern Gawler Craton (*e.g.* Fraser & Lyons, 2006; Morrissey *et al.*, 2019). Drill holes on the Yorke Peninsula contain *ca* 1556–1546 Ma granites based on laser ablation-inductively coupled plasma mass spectrometry (LA-ICPMS) zircon U–Pb dating (Reid, Zhou, *et al.*, 2020). These dates are similar to ages obtained from granites in the Peake and Denison inliers of the northeastern Gawler

Craton (Fanning et al., 2007). The ca 1565–1450 Ma events are widely distributed across the Gawler Craton; however, the timing and causes of geological activity at this time are not well understood.

Subsequent to these early Mesoproterozoic events, the Gawler Craton was variably buried by a series of sedimentary basins, including the Carriwerloo Basin (Fanning et al., 1983) and Neoproterozoic to Cambrian rocks of the Adelaide Superbasin (Lloyd et al., 2020). On the Yorke Peninsula where this study has been undertaken, sedimentary rocks of Cambrian, Permian, Eocene and Plio-Pleistocene age are present and largely obscure the crystalline basement geology, except for excellent coastal exposures (Zang, 2006).

Field relationships of mafic dykes, Southern Yorke Peninsula

Mafic dykes on Southern Yorke Peninsula have sharp, cross-cutting contacts with host gneisses and form dykes that range from ~0.5 to 8 m wide (Figure 4a). These straight-sided dykes are composed of hornblende–plagioclase–biotite ± clinopyroxene ± quartz, and some examples retain primary igneous textures (Zang, 2006). We term this set of mafic dykes the Daly Head Metadolerite (see definition in Appendix 1). Smaller dykes, <1 m, tend to display finer grainsize adjacent to the contact with the country rock that may reflect chilled margins. Larger dykes, >5 m wide, display a weak alignment of amphibole and/or biotite that is typically parallel to the dyke margins, although the central portions of these dykes, such as the one sampled for geochronology, are coarser grained, and has a less pronounced mineral alignment/foliation (Figure 4b). The sampled metadolerite from Royston Head (Figure 5), contains clinopyroxene that is partly retrogressed to amphibole, likely cummintonite–grunerite, and is intergrown with medium-grained plagioclase and dynamically recrystallised, equant grains of quartz (Figure 4c). Brown biotite defines the mineral foliation and plagioclase is partly retrogressed to white mica.

Several of the larger Daly Head Metadolerite dykes at the Royston Head locality are deformed by narrow shear zones, including the particular dyke sampled for zircon geochronology. The shear zone that cuts the dated dyke at Royston Head is < 2 m wide and resulted in reorientation of amphibole–biotite within the mafic dyke (Figure 4d, e). In addition, this shear zone also affects the gneissic foliation within the granite of the Donington Suite (Figure 4f). Within the gneiss, this shear zone is characterised by stretching and recrystallisation of quartz and feldspar and the reorientation of the gneissic foliation. The shear zone trends approximately orthogonally to the mafic dyke and can be traced for tens of metres within felsic gneiss. In one area, the shear zone contains a ~10 cm wide granite dyke, orientated parallel to the shear zone margins and showing a weak mineral alignment, suggesting this granite sheet

was emplaced during the development of the shear zone (Figure 4e). Reid et al. (2008) identified similar shear zones as being the latest phase of ductile deformation during the Cornian Orogeny; however, no definitive geochronology was then available to show this was the case.

Dykes of the Daly Head Metadolerite that cut the gneissic fabric of the Donington Suite on the Yorke Peninsula are lithologically and texturally distinct from other mafic rocks exposed in the area known as the Jussieu Metadolerite. Mafic rocks of the Jussieu Metadolerite are co-magmatic with and petrogenetically linked to the Donington Suite, and are not cross-cutting (Schwarz, 2003; Zang, 2006). Previous regional mapping by the Geological Survey of South Australia had correlated the Daly Head Metadolerite dykes with a set of ca 1810 Ma mafic dykes exposed on coastal outcrops on the Eyre Peninsula known as the Tournefort Metadolerite (Zang, 2006). However, our new data suggest this correlation is incorrect.

In this study, a sample (698213) was collected from the centre of a large mafic dyke for zircon U–Pb geochronology using sensitive high-resolution ion microprobe (SHRIMP; location map Figure 5). To complement this geochronology, a series of samples of similar cross-cutting mafic dykes in the southwestern Yorke Peninsula were analysed for whole-rock geochemistry (Table 1). A subset of four samples were analysed for their Sm–Nd isotopic composition to investigate their petrogenesis. In addition, to determine the age of this granitic intrusion, a sample (1893814) was also collected of the narrow granite sheet that cross-cuts the mafic dyke and intrudes the late-stage shear zone. This sample was analysed via zircon U–Pb geochronology using laser ablation-inductively coupled plasma mass spectrometry (LA-ICPMS).

Analytical methods

Details of analytical methods are provided in the Supplemental Data and briefly summarised as follows. Zircons from the samples were mounted in epoxy resin, polished, and imaged under plain transmitted and reflected light and with cathodoluminescence (CL). U–Pb isotopic analyses on the sample from the mafic dyke were undertaken using sensitive high-resolution ion microprobe (SHRIMP) using the SHRIMP IIe at Geoscience Australia in Canberra. Established SHRIMP operating procedures and data reduction schemes were used (Williams, 1998). Temora 2 zircon standard (416.8 ± 0.3 Ma; Black et al., 2004) was used to monitor differential fractionation between U and Pb, and isobaric interference at the ^{204}Pb mass peak. The OG1 reference zircon (Stern et al., 2009) was used to monitor ^{207}Pb/^{206}Pb reproducibility and accuracy, and produced an age of 3464.8 ± 2.3 Ma for the session (MSWD = 1.3). Correction for non-radiogenic Pb in zircon was based on the measured ^{204}Pb/^{206}Pb and a contemporaneous Pb isotope composition determined according to Stacey and
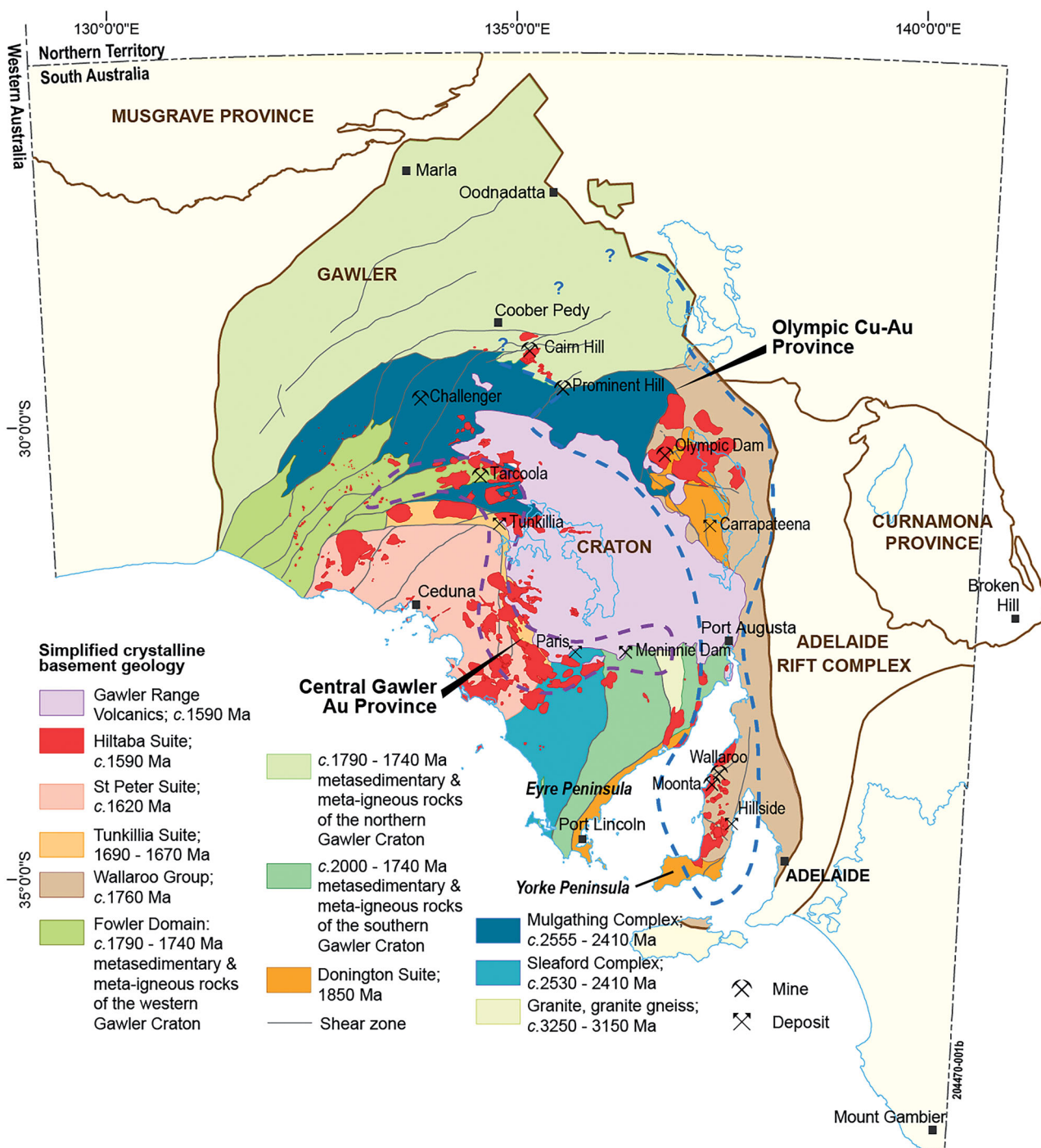
Figure 1. Simplified solid geology of the Gawler Craton (after Reid & Fabris, 2015). The location of the Donington Suite in the eastern Gawler Craton is shown along with the extent of the early Mesoproterozoic Hiltaba Suite and Gawler Range Volcanics magmatism. Olympic Cu–Au Province and Central Gawler Gold province outlines modified from Skirrow *et al.* (2007) and Budd and Fraser (2004), respectively.

Kramers (1975). Squid-2 software was used for data reduction (Ludwig, 2009).

LA-ICPMS analysis was undertaken at Adelaide Microscopy, University of Adelaide, and utilised a New Wave 193 nm laser coupled to a New Wave Research Nd–YAG laser with a 30 μm spot size coupled to an Agilent 7500 quadrupole ICPMS using methodology documented by Howard *et al.* (2011). Time-resolved signals of [204, 206,]

[207, 208]Pb, [232]Th and [238]U were acquired with a 5 Hz repetition rate and processed using GLITTER software (Griffin *et al.*, 2008). The GJ-1 standard zircon (Jackson *et al.*, 2004) was used to calibrate U and Pb fractionation, and data quality was monitored by analysing zircon standards QGNG (1851.6 ± 0.6 Ma; Black *et al.*, 2003) and Plešovice (337.13 ± 0.37 Ma; Sláma *et al.*, 2008). Weighted mean ages for these standards during the analysis of sample 1893814
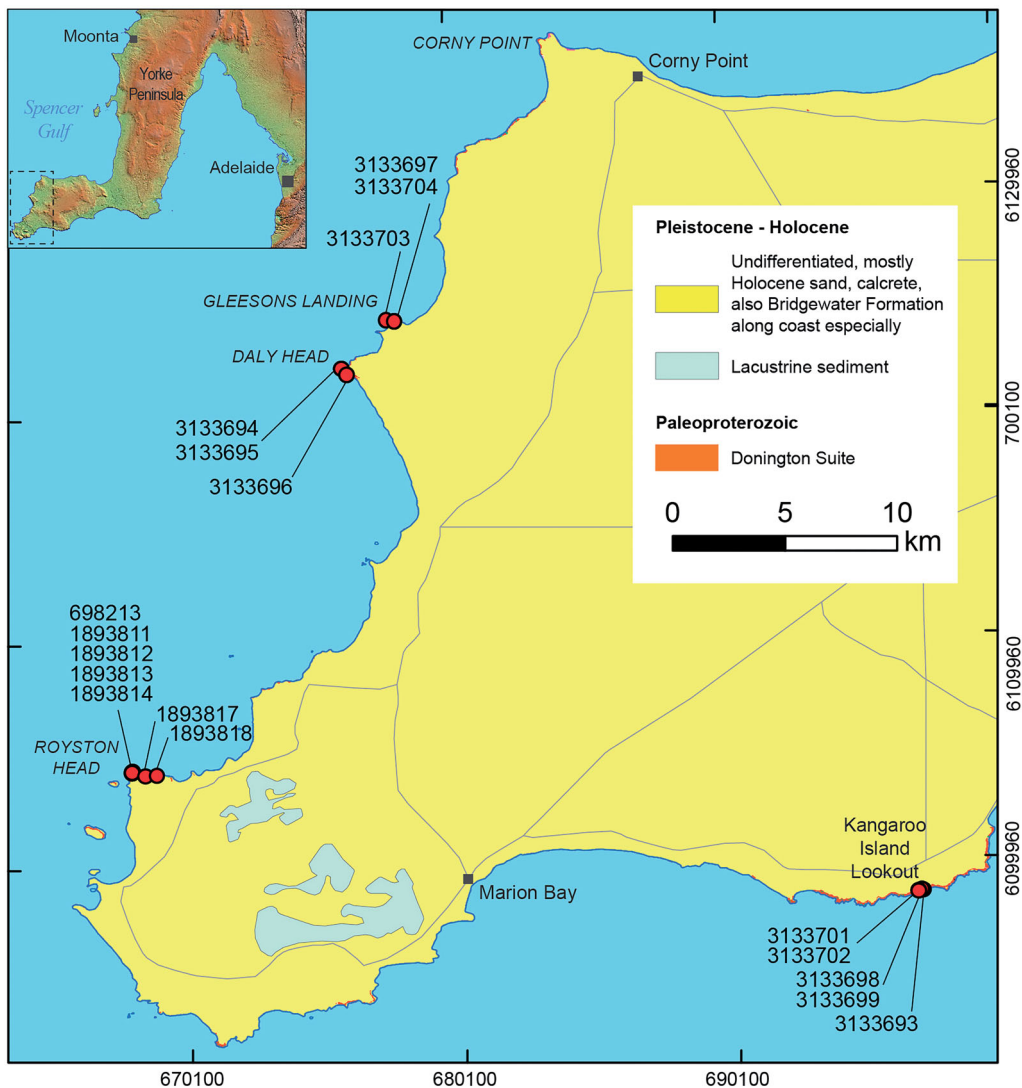
Figure 2. Location of samples presented in this study on a simplified surface geology map of the southwestern Yorke Peninsula. Note that Donington Suite outcrop is limited to narrow coastal zones. Outcrop of Daly Head Metadolerite is limited and does not appear at the scale of this map. Inset shows the location of the Yorke Peninsula relative to Adelaide.

were 1840 ± 22 Ma ([207]Pb/[206]Pb age, n = 4, MSWD = 0.74) and 342 ± 13 Ma ([206]Pb/[238]U age n = 4; MSWD = 2.7), respectively. The LA-ICPMS data for [204]Pb are compromised by interference from [204]Hg, a trace contaminant in the Ar–He carrier gas and by the low detection levels. No correction for non-radiogenic Pb has been applied to the LA-ICPMS data. Age calculations for both SHRIMP and LA-ICPMS data were made using Isoplot/Ex (Ludwig, 2003). Isotopic ratios and single ages are cited at $\pm 1\sigma$, whereas weighted mean [207]Pb/[206]Pb ages are given at 95% confidence limits.

Geochemical analyses for samples 1892810–1893181 were performed by ALS, Perth, Western Australia. Major elements were analysed using ICP-AES. Trace elements were determined by LA-ICP-MS. Geochemical analyses for samples 3133690–3133699 and 3133701–3133704 were performed by BV Minerals in Perth, WA. Major elements and

chlorine were analysed by X-Ray Fluorescence spectrometry. Trace elements were determined by laser ablation-inductively coupled plasma mass spectrometry (LA-ICP-MS), and Au, Pt and Pd were analysed using fire assay ICP-MS. FeO was determined volumetrically and fluorine was determined using specific ion electrode.

Sm–Nd isotope analyses were performed at the University of Adelaide following the method of Wade et al. (2006). Nd analyses were conducted using a Finnigan MAT262 thermal ionisation mass spectrometer, in static and quadruple-cup dynamic measurement modes, normalised to $^{146}/^{144}$Nd = 0.721903 and Nd concentrations corrected for 200 pg blank. Sm analyses were carried out on a Finnigan MAT262 thermal ionisation mass spectrometer, in static mode, and Sm concentrations were corrected for 150 pg blank. The average measured ^{143}Nd/^{144}Nd ratio for the G-2 standard (United States Geological Survey granitic
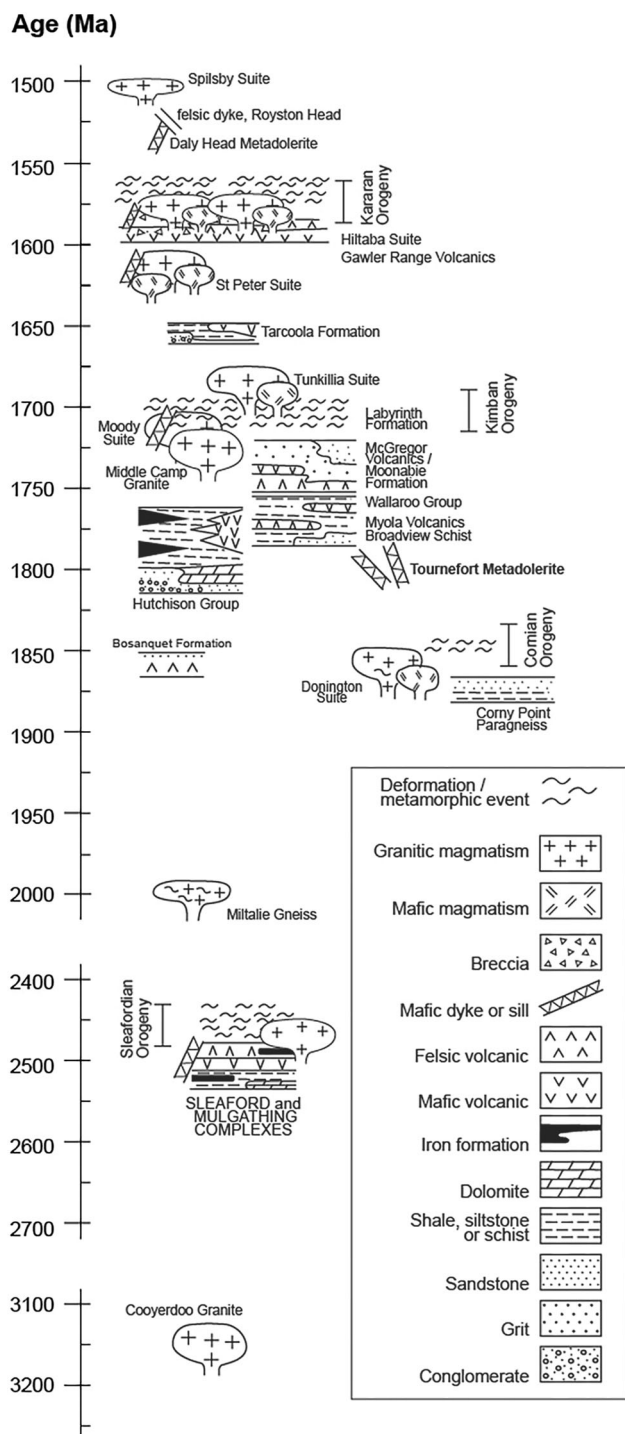
Age (Ma)

Figure 3. Simplified stratigraphic column of the southern Gawler Craton. Modified from Reid and Fabris (2015).

reference material) is 0.512212 ± 0.00002 ($n = 5$), comparable with the GeoRem preferred value (0.512233 ± 0.00001; http://georem.mpch-mainz.gwdg.de/start.asp?dataversion=current). Calculated concentrations for Nd and Sm in G-2 are 52.78 ppm and 7.55 ppm, respectively, compared with the GeoRem preferred values of 53.81 ± 0.67 ppm and 7.91 ± 0.1 ppm, respectively. All geochemical and isotopic data are provided in online data files.

Geochronology results

Mafic dyke sample 698213 yielded abundant small, 40–100 μm-sized zircons. The zircons are clear, colourless crystals with equant to low aspect ratio (Figure 6a). Most zircons have irregular, somewhat angular, partially developed crystal faces. Few of the zircons have pyramidal terminations. Under CL, around half of the zircons have complex core–rim structures with cores of low CL response and therefore dark zircon surrounded by lighter CL response rims. Some of the zircons with these lower CL response cores have patches of very high CL response adjacent to the cores. The remainder of the zircon grains are composed entirely of moderate or light grey CL response zones that are either homogenous or broadly zoned.

All SHRIMP analyses are concordant to subconcordant and only one grain contains significant common Pb (Figure 7a). The majority of analyses have Th/U values between 0.84 and 0.10, with outliers having a high value of 1.34 and lower value of 0.05. The low CL response zircon cores have ages that cluster at *ca* 1770 Ma; 14 analyses yield a weighted mean $^{207}Pb/^{206}Pb$ age of 1770 ± 6 Ma (MSWD = 1.4). One oscillatory-zoned grain records an age of *ca* 1860 Ma. Analyses of the homogenous, dark CL crystals and zircon rims cluster at *ca* 1565 Ma. Omitting the three youngest analyses as outliers possibly reflecting subtle Pb loss, the remaining 21 analyses produce a weighted mean $^{207}Pb/^{206}Pb$ age of 1564 ± 4 Ma (MSWD = 1.4). Outside these two groups, there are 23 analyses with apparent ages ranging between *ca* 1752 and *ca* 1583 Ma. These analyses appear to have inadvertently straddled core–rim boundaries and likely represent isotopically mixed compositions between the older and younger zircon.

Sample 1893814 is from the 10 cm wide granitic dyke that cuts the gneissic foliation within Donington Suite orthogneiss and mafic dyke. Zircons from this sample are mostly dark in colour with dark CL response that is indicative of radiation damage likely owing to high U content (Figure 6b). Where the grains are less dark in transmitted light, the CL response is also brighter and generally oscillatory-zoned, suggesting a magmatic origin. The data are affected by a combination of Pb loss and non-radiogenic Pb, as indicated by variable discordance (Figure 7b). Omitting the most discordant analyses (3814-08, 3814-12, 3814-14, 3814-03, 3814-04) and two analyses that are anomalously old (3814-02, 3814-05), the remaining analyses cluster at around *ca* 1555 Ma. A weighted mean $^{207}Pb/^{206}Pb$ age of 1554 ± 8 Ma can be calculated; however, there is significant scatter in the data (MSWD = 8, $n = 14$). Nevertheless, the *ca* 1555 Ma age likely approximates the timing of igneous crystallisation of the syn-kinematic granite sample.

Whole-rock geochemical and isotopic results

To describe the geochemical results obtained in this study, we divide the samples into two groups. The first is a subset
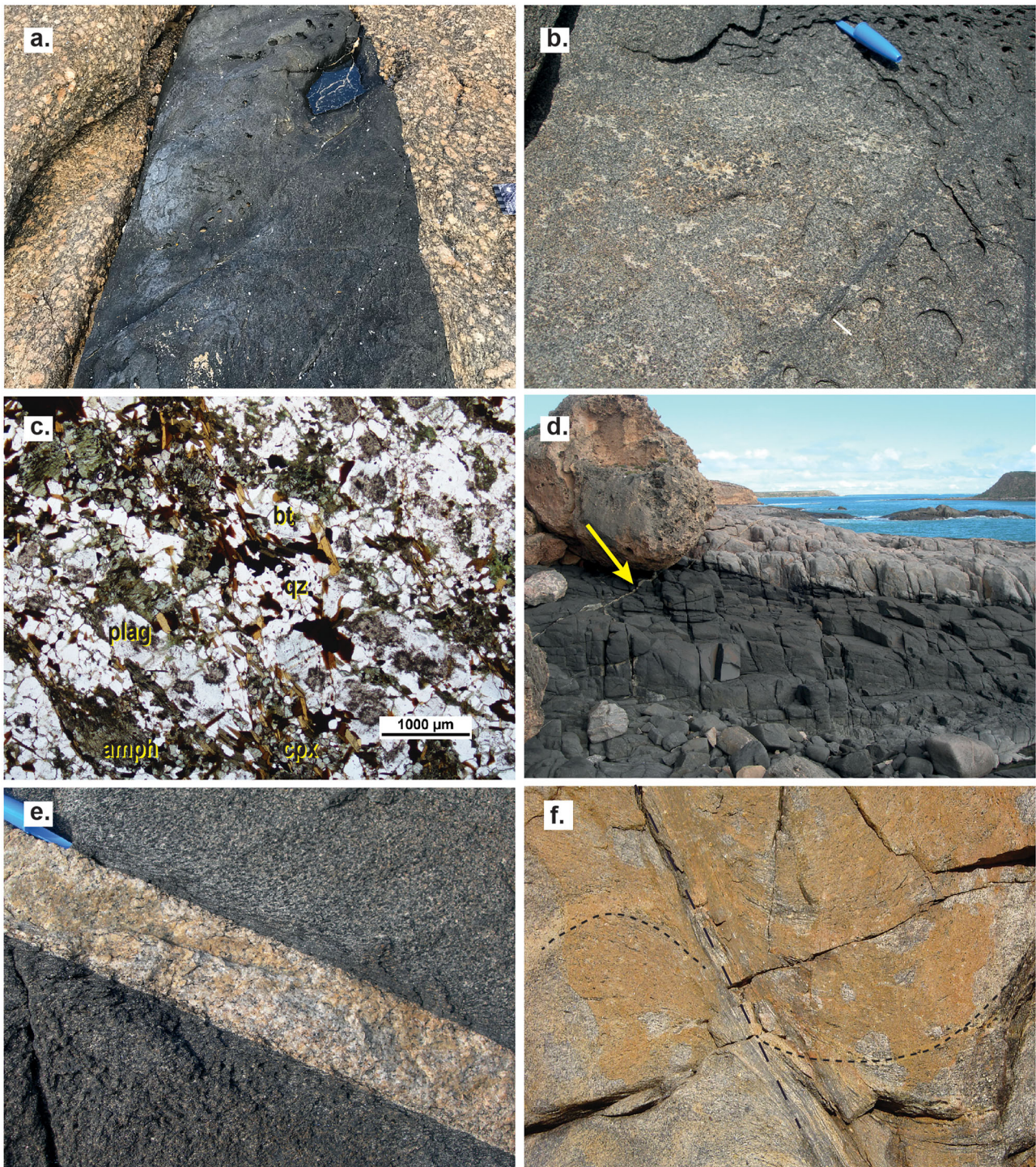
Figure 4. Field photographs of Daly Head Metadolerite and cross-cutting shear zone from Southern Yorke Peninsula. (a) Example of straight-sided mafic dyke, typical of Daly Head Metadolerite, that cuts augen-textured megacrystic granite of the Donington Suite. Berry Bay locality, approximate location: Lat. −34.922, Long. 137.010. (b) Detail of texture within metadolerite dyke from which sample 698213 was taken. Note coarse plagioclase + quartz indicating a more fractionated component to the mafic rock. Pen lid is approximately 2.5 mm wide. Location, Royston Head, Yorke Peninsula. Lat. −35.1911, Long. 136.8464. (c) Thin-section photomicrograph of sample 698213. Clinopyroxene (cpx) occurs within a dynamically recrystalised plagioclase (plag) + quartz (qz) matrix. Clinopyroxene is partially replaced by amphibole (amph, likely actinolite) and plagioclase by white mica. Biotite (bt) is preferentially aligned and helps to define a solid-state fabric within the sample. (d) View across Daly Head Metadolerite dyke from which sample 698213 was taken, looking to the southwest. Note the narrow granitic vein, indicated with yellow arrow, that crosscuts the trend of the dyke and adjacent Donington Suite gneisses. This granitic vein is the same vein from which sample 1893814 was taken. Note large boulder of Plio-Pleistocene Bridgewater Formation calc-arenite, typical of the cover sequence that overlies the Donington Suite in the region. Location, Royston Head. Lat. −35.1911, Long. 136.8464. (e) Detail of contact between sampled granitic dyke (sample 1893814) and weak mineral foliation within metadolerite dyke shown in (f). Note the deflection of the foliation about the intrusion. Pen lid is approximately 2.5 mm wide. Location, Royston Head. Lat. −35.1911, Long. 136.8464. (f) Example of narrow, ductile shear zone that reworks Donington Suite orthogneiss. This shear zone has an apparently normal sense of shear; foliation within orthogneiss is indicated by short, dashed lines. Orientation of shear zone itself indicated by long dashed line. View is looking east, and pen for scale is 14 cm long. Location, Royston Head. Lat. −35.1916, Long. 136.8571.
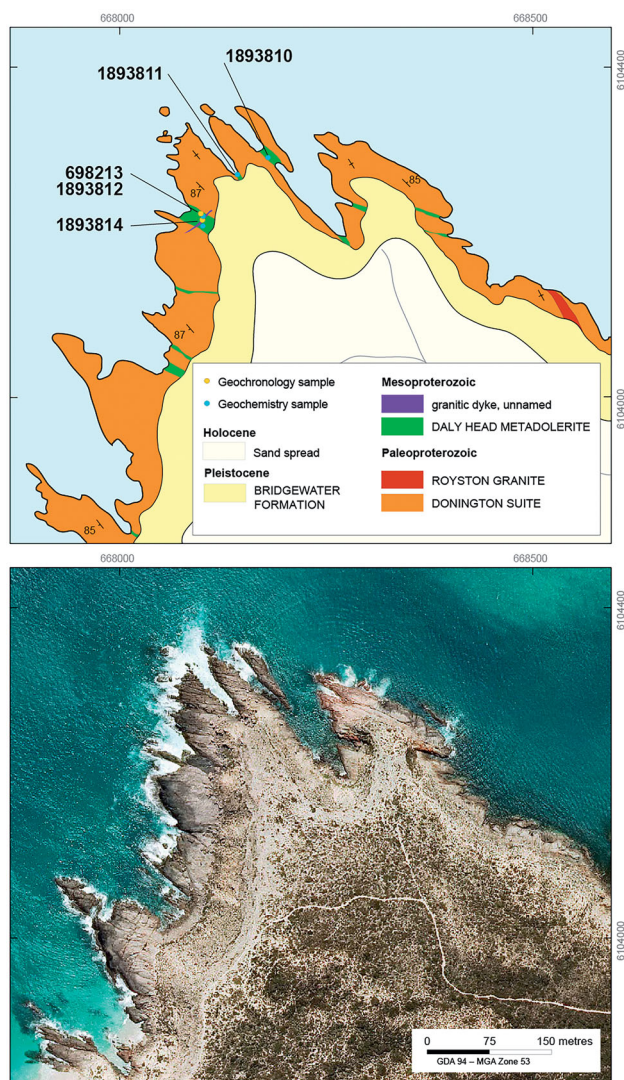
Figure 5. Geological map of Royston Head, southeastern Yorke Peninsula, showing the location of geochronology samples. Lower panel shows orthoimagery of the Royston Head locality.

of analyses from samples at the Royston Head locality, of which we are confident that these dykes are *ca* 1564 Ma in age. We call these 'Royston Head mafic dykes' in the following section. We then compare the data obtained from this locality with data from mafic dyke samples from other localities on Southern Yorke Peninsula, which we refer to as 'Southern Yorke Peninsula mafic dykes'. Note that the results suggest that these two subdivisions are arbitrary and that the entire set can be grouped into a single unit, the Daly Head Metadolerite. Nevertheless, to objectively examine their similarity, we keep the two groups separate in this section.

Royston Head mafic dykes

Mafic dyke samples from Royston Head display similar variation in major elements, with low SiO_2 (46.6–50.7 wt%), low alkali contents ($Na_2O + K_2O$ wt%), low to moderate MgO

contents (3.6–6.87 wt%) and high Fe_2O_{3T} contents (12.05–18.65 wt%). These dykes correspond to gabbro on the total alkali silica (TAS) diagram and tholeiites on the AFM ($Na_2O + K_2O$–FeO_{tot}–MgO) diagram (Figure 8). Significant variation is observed in Mg# (28–53) in the Royston Head mafic dykes (Mg# calculated as molar Mg# = (Mg/[Mg + Fe] x100)), although moderate values between 38 and 46 are most common. Small variations are seen in the major elements TiO_2 (0.96–2.85 wt%), Al_2O_3 (13.5–15.3 wt%), CaO (8.15–10.8 wt%) and P_2O_5 (0.09–0.29 wt%). The major elements CaO and Al_2O_3 increase with increasing MgO, and TiO_2, Fe_2O_{3T}, P_2O_5 and SiO_2 decrease with increasing MgO (Figure 9). Cr and Ni contents in Royston Head mafic dykes are low (Cr = 30–140 ppm and Ni = 46–105 ppm), and Cr forms a positive correlation with increasing MgO (Figure 9). Negative correlations are formed between Zr and Ce and Nb (not shown) with respect to MgO (Figure 9).

Large ion lithophile elements Rb, Ba, Th, U and K display significant variation on primitive mantle-normalised trace element plots (Figure 10a). Trace element patterns are characterised by negative Nb, Sr and P anomalies and negative Ti anomalies are insignificant (Figure 10a). The trace element patterns and abundance are similar to global subducting sediment (GLOSS) and bulk crust patterns, excepting the absence of pronounced negative Ti anomalies (Figure 10a). A subset of Royton Head mafic dykes has trace-element patterns that more closely resemble E-MORB, which are characterised by lower large ion lithophile element (LILE), La, Ce, Pr and higher heavy rare earth elements (REEs) than bulk crust (Figure 10a).

REE abundances are low (total REE = 59–152.8 ppm) and show a slight enrichment in light REE (LREE) over HREE (($La/Yb)_N$ = 2.66–7.44). Eu anomalies are insignificant, presenting as weakly negative to weakly positive (Eu/Eu* = 0.86–1.13). LREE abundance for Royston Head mafic dykes generally range between GLOSS and E-MORB values, while medium to HREE are more enriched than GLOSS and E-MORB (Figure 10b).

Sm–Nd isotopic data from four samples have $\varepsilon_{Nd(1560\,Ma)}$ values of −6.8 to −2.9 (Table 2). Ancient, depleted mantle model ages (T_{DM}) are calculated for the Royston Head mafic dykes, which are mostly *ca* 2.9–2.5 Ga, although one sample has a T_{DM} age of 4.2 Ga (Table 2).

Southern Yorke Peninsula mafic dykes

Straight-sided mafic dykes of the Southern Yorke Peninsula have major element compositions comparable with the Royston Head mafic dykes (Figures 8–10). Southern Yorke Peninsula mafic dykes are classified as gabbro on the TAS diagram (Figure 8a). The majority of the Southern Yorke Peninsula samples are tholeiite with three samples transitional to calc-alkaline series (Figure 8b). Southern Yorke Peninsula mafic dykes have low SiO_2 contents in a similar range to the Royston Head mafic dykes (46.8–50.9 wt%)

Table 1. Details of samples analysed in this study.

Sample	Lithology	Location	Easting	Northing	Zone	Analysis
698213	Metadolerite	Royston Head	669483	6104041	53	SHRIMP zircon U–Pb
1893814	Granite	Royston Head	668111	6104202	53	LA-ICPMS zircon U–Pb
1893810	Metadolerite	Royston Head	668153	6104287	53	Whole-rock geochemistry
1893811	Metadolerite	Royston Head	668114	6104261	53	Whole-rock geochemistry, Sm–Nd isotopes
1893812	Metadolerite	Royston Head	668111	6104203	53	Whole-rock geochemistry, Sm–Nd isotopes
1893813	Metadolerite	Royston Head	668121	6104211	53	Whole-rock geochemistry, Sm–Nd isotopes
1893817	Metadolerite	Royston Head	668602	6104048	53	Whole-rock geochemistry, Sm–Nd isotopes
1893818	Metadolerite	Royston Head	669040	6104082	53	Whole-rock geochemistry
3133693	Metadolerite	Kangaroo Island Lookout	696924	6098456	53	Whole-rock geochemistry
3133694	Metadolerite	Daly Head	676119	6122085	53	Whole-rock geochemistry
3133695	Metadolerite	Daly Head	676119	6122085	53	Whole-rock geochemistry
3133696	Metadolerite	Daly Head	676302	6121823	53	Whole-rock geochemistry
3133697	Metadolerite	Gleeson's Landing	678087	6124158	53	Whole-rock geochemistry
3133698	Metadolerite	Kangaroo Island Lookout	696876	6098484	53	Whole-rock geochemistry
3133699	Metadolerite	Kangaroo Island Lookout	696876	6098484	53	Whole-rock geochemistry
3133701	Metadolerite	Kangaroo Island Lookout	696763	6098418	53	Whole-rock geochemistry
3133702	Metadolerite	Kangaroo Island Lookout	696763	6098413	53	Whole-rock geochemistry
3133703	Metadolerite	Gleeson's Landing	677807	6124227	53	Whole-rock geochemistry
3133704	Metadolerite	Gleeson's Landing	678088	6124160	53	Whole-rock geochemistry
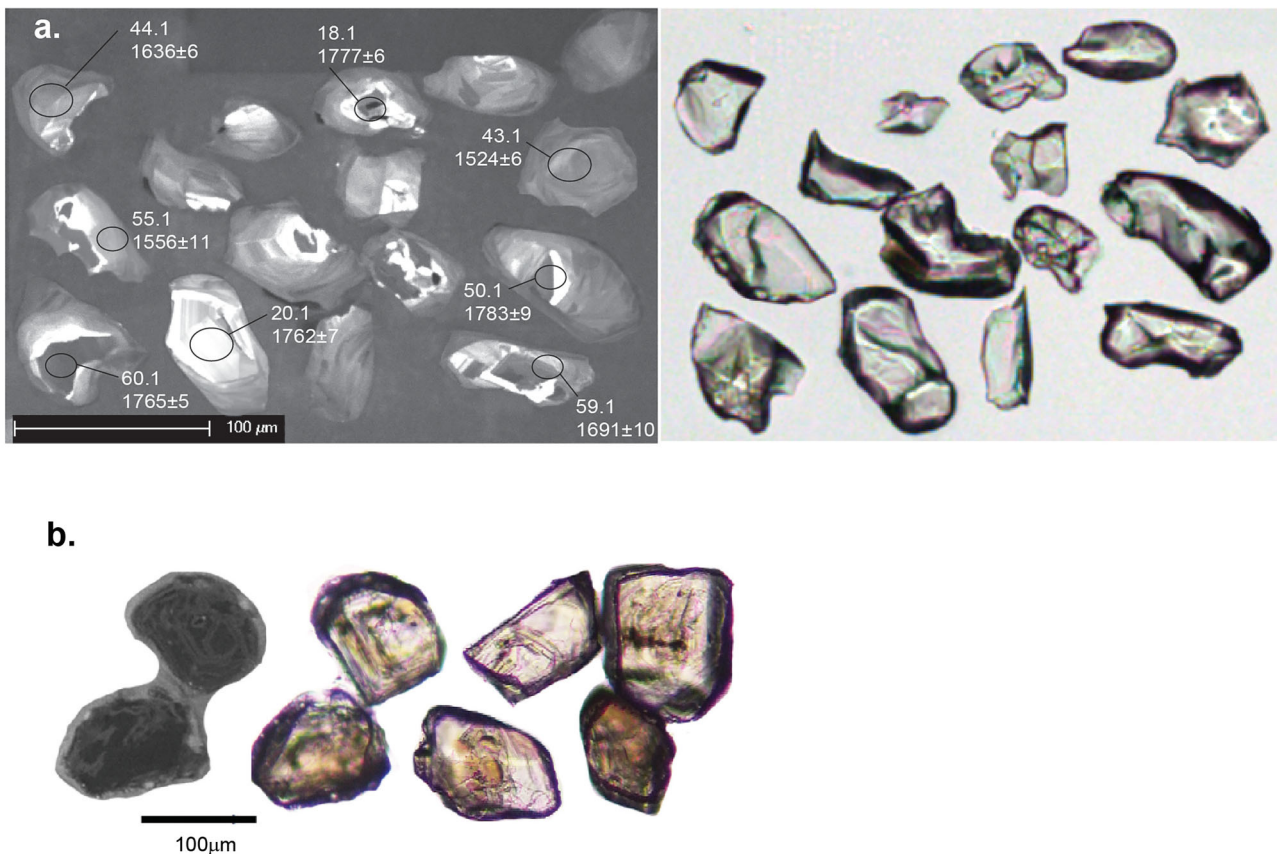
Figure 6. Representative images of zircons from samples analysed in this study. (a) Cathodoluminescence image of zircons from sample 698213 showing the clear core–rim structure to the zircons. (b) Cathodoluminescence and transmitted light image of zircons from sample 1893814.

and slightly higher MgO contents relative to the Royston Head mafic dykes (MgO = 5.6–7.9 wt%). Mg# range from 39 to 58 in the Southern Yorke Peninsula mafic dykes, comparable with the Royston Head gabbro Mg# (28–53). Variations in the major elements Fe_2O_{3T} (11.2–16.9 wt%), TiO_2 (0.81–2.14 wt%), Al_2O_3 (13.3–15.6 wt%), CaO (8.1–11.9 wt%) and P_2O_5 (0.08–0.3 wt%) are similar to the Royston Head mafic dykes (Figure 9). The major elements CaO and Al_2O_3 increase with increasing MgO, however the Southern Yorke Peninsula mafic dykes form a separate parallel positive correlation between Al_2O_3 and MgO compared with the Royston Head mafic dykes (Figure 9). TiO_2, Fe_2O_{3T}, P_2O_5 and SiO_2 decrease with increasing MgO (Figure 9). Cr and Ni are low to moderate in the Southern Yorke Peninsula mafic dykes (Cr = 32–260 ppm and Ni = 49–130 ppm) but extend to higher values when compared with mafic dykes from Royston Head. Trace elements such as Zr, Ce and Nb (not shown) are similar in abundance and
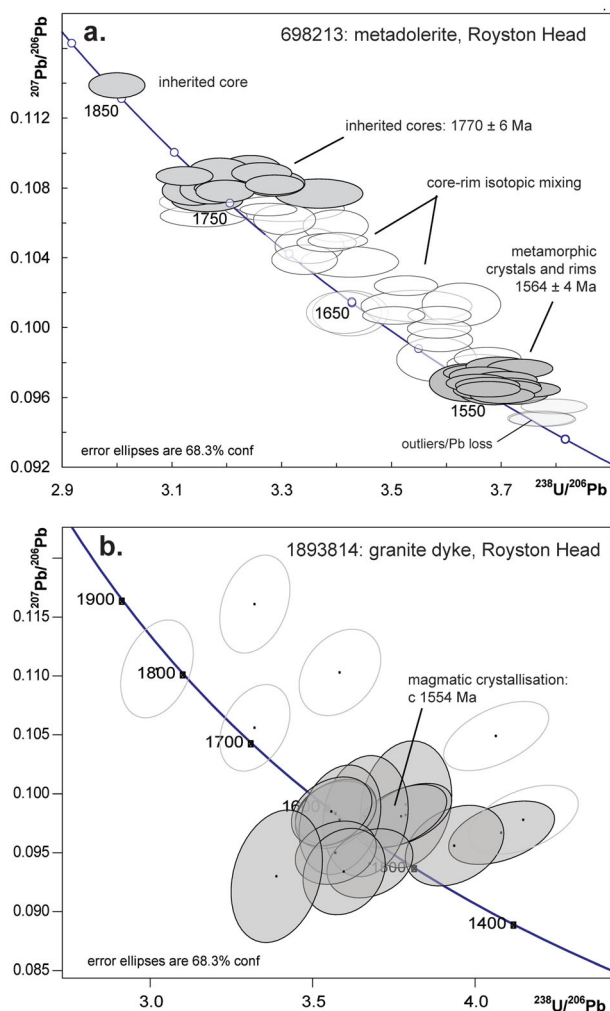
Figure 7. Tera-Wasserburg Concordia diagrams for samples (a) 698213 and (b) 1893814. Colouring of analytical ellipses is according to the geological interpretation of the analyses as indicated by the ages.

form the same negative correlations with MgO as the Royston Head mafic dykes (Figure 9).

Primitive mantle-normalised trace element patterns show that these mafic dykes from Southern Yorke Peninsula are similar to those from Royston Head, supporting stratigraphic correlation between the two. These patterns are typified by large variations in Rb, Ba, Th, K and U, negative P anomalies, and similar abundances of high-field-strength elements and REEs (Figure 10a). The Southern Yorke Peninsula mafic dykes differ in their trace element patterns to the Royston Head mafic dykes by the presence of coupled negative Nb–Ta anomalies, and slightly larger negative Ti anomalies (Figure 10a). Southern Yorke Peninsula mafic dykes have low profile REE patterns, with small LREE enrichment to HREE ($(La/Yb)_N$ = 1.79–6.11). LREE variation is also apparent in the Southern Yorke Peninsula gabbro samples compiled from Reid *et al*. (2008). Similar abundances of medium to HREE are seen in the Southern Yorke Peninsula mafic dykes and Royston Head mafic dykes (Figure 10b).

Discussion

Geochronological interpretation: age of mafic dyke and implications for magmatic style and regional geology of the southern Gawler Craton

Zircons from the mafic dyke sample yield two broad age populations. The youngest is a population at 1564 ± 4 Ma and corresponds to zircons with light grey, higher CL response as both rims on grains with core–rim structure and whole grains with similar light grey, higher CL response. The older ages at 1770 ± 5 Ma and *ca* 1860 Ma are derived from the dark, low CL response cores. The simplest interpretation of these data is that 1564 ± 4 Ma represents the timing of magmatic crystallisation of the mafic dyke. This interpretation is supported by the morphology of the zircons, which are mainly anhedral with irregular shapes, some having narrow, elongate protuberances extending from the crystal faces. These textures can be interpreted as having formed owing to zircon crystallisation interstitial to already formed crystals, such as plagioclase or pyroxene during igneous formation of the mafic dyke. Textures reminiscent of these are observed in other mafic dykes and gabbroic suites (*e.g.* Teng & Santosh, 2015; Wingate *et al*., 1998; Zang *et al*., 2007). In addition, the presence of whole grains with light grey, higher CL response and ages in the *ca* 1564 Ma population is suggestive of these grains having formed during igneous crystallisation. We note also that Th/U ratios from the zircons in the mafic dyke sample average ∼0.25, which is more similar to Th/U ratios from magmatic rocks (Hoskin & Schaltegger, 2003; Kirkland *et al*., 2015) compared with the generally lower Th/U ratios, <0.05, typically found in metamorphic zircon (Rubatto, 2002).

If the interpretation that the mafic dyke was emplaced at 1564 ± 4 Ma were correct, this would imply that the older ages derived from zircon cores are inherited zircon. There are two aspects to consider regarding the interpretation of inherited zircons in this mafic dyke. The first is how a mafic magma can both retain inherited zircon and crystallise new zircon. The second is the implications of the ages of these inherited zircons for the overall regional geological evolution of the Gawler Craton.

Variables that affect zircon dissolution in magmatic rocks include the composition and temperature of the magma, the size of xenocrysts and the rate of magmatic cooling. In general, mafic magmas are high temperature, with basaltic liquid in modern settings being 1200–1400 °C (*e.g.* Lee *et al*., 2009). Such temperatures should be enough to dissolve zircon, particularly if the magma is Zr undersaturated to begin with and noting some dependence on the major element chemistry of the magma (*e.g.* Shao *et al*., 2019; Watson & Harrison, 1983). Experimental studies that demonstrate more efficient zircon dissolution in higher-temperature magmas are supported by field studies such as that of Bhattacharya *et al*. (2018) from arc batholiths of Fiordland, New Zealand. Their study showed that
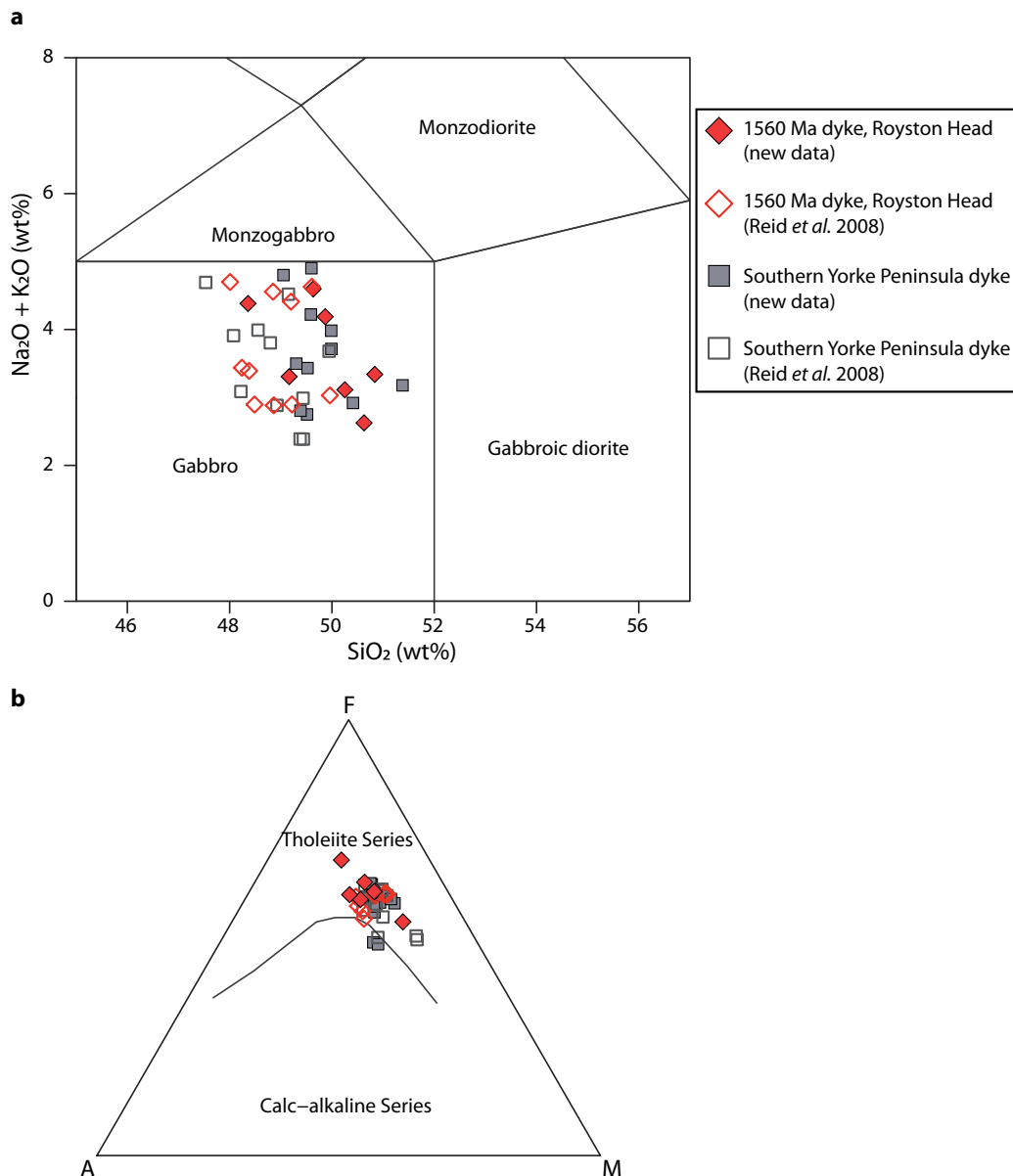
Figure 8. Geochemical classification diagrams for Daly Head Metadolerite. In this plot, and in other geochemical diagrams to follow, we separate Daly Head Metadolerite mafic dyke samples from the Royston Head locality from those elsewhere on Southern Yorke Peninsula. (a) Total alkali silica (TAS) classification diagram after Middlemost (1994). (b) Alkali–iron–magnesium (AFM) classification plot of Irvine and Baragar (1971).

dykes with temperatures >850 °C dissolved inherited zircon more effectively than lower-temperature magmas. While magmatic temperature is a primary control, Farina *et al.* (2014) have shown that smaller zircons will dissolve more readily in a magma than large ones, and faster cooling magmas will dissolve less zircon than slowly cooled magmas. Therefore, in order to retain xenocrystic zircons, mafic magmas need to either be relatively cool or crystallise rapidly, and the zircons themselves need to be relatively large.

In the case of the mafic dyke in this study, xenocrystic zircon cores range in size from ∼30 μm in long axis to ∼80 μm in length (Figure 7), which is in the order of the size of zircon modelled by Farina *et al.* (2014) as being able to survive in magmas of temperature 825 °C if cooling of the magma occurred over a period of time less than

approximately 8000 years. Therefore, although mafic in composition and likely to have had initially high magmatic temperatures, the mafic dyke sampled in this study must have cooled relatively rapidly following incorporation of the xenocrystic zircons. The presence of inherited zircon suggests either that the magma was of a temperature below zircon stability or, perhaps more likely, that the time between entrainment of the xenocryst and crystallisation of the magma was not sufficient to allow total dissolution of zircon. Furthermore, assuming the mafic magma was Zr undersaturated, pre-existing xenocryst grain boundaries are likely sites of lower free energy that permit nucleation of new zircon growth. The fact that many of the zircons analysed from this dyke contain older cores supports this inference.
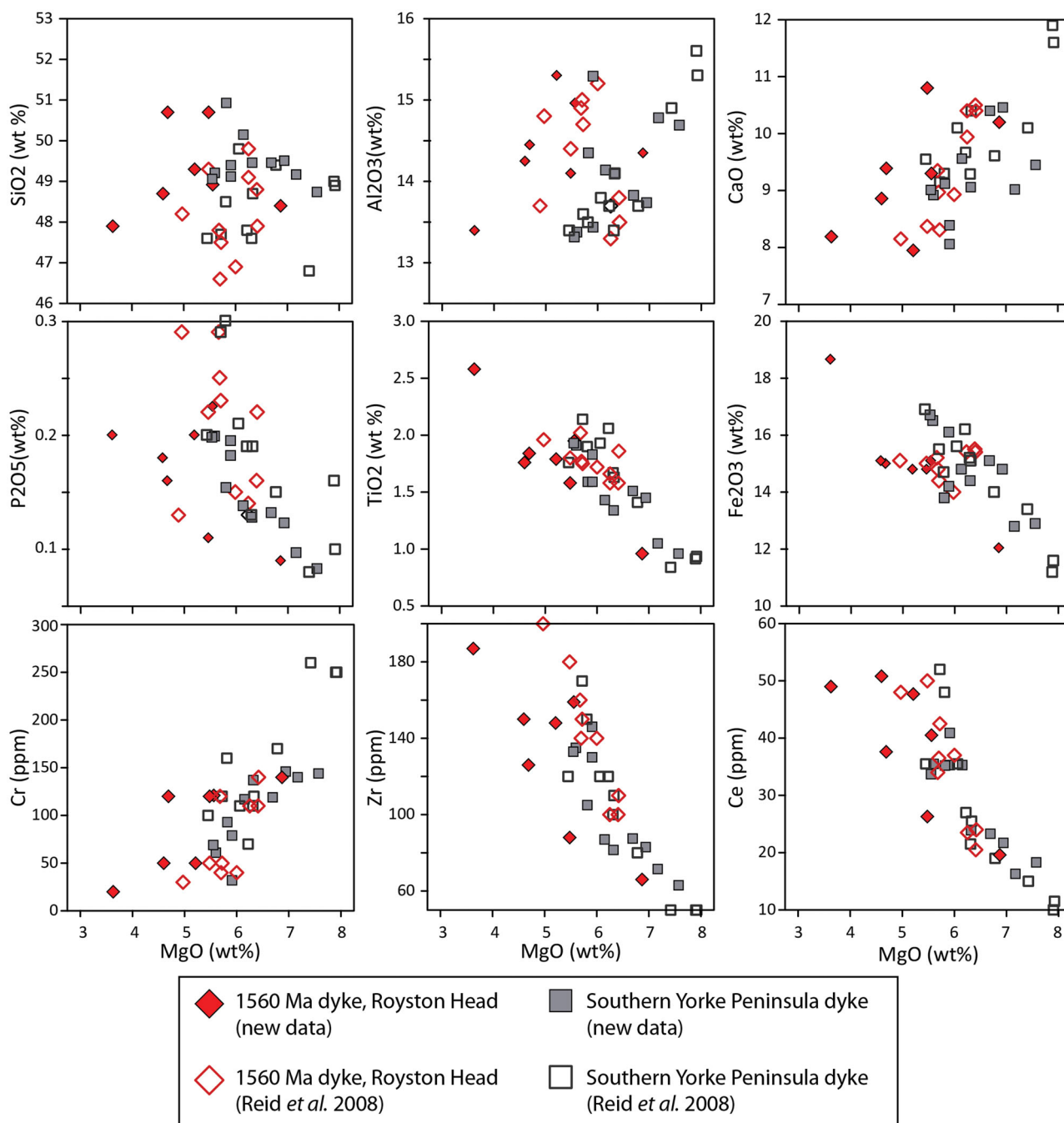
Figure 9. Plots of selected elements *vs* MgO for Daly Head Metadolerite subdivided into the Royston Head mafic dykes and Southern Yorke Peninsula mafic dykes.

These inherited zircons have a population at 1770 ± 6 Ma and a single analysis with an age of *ca* 1860 Ma. Clearly, the *ca* 1860 Ma zircon is derived from the adjacent Donington Suite. The *ca* 1770 Ma population is likely to be derived from magmatic rocks that occur beneath the current exposure level. Magmatism of this age is present elsewhere on the Yorke Peninsula, in particular, the Wardang Volcanics, which were erupted at 1772 ± 14 Ma and are part of the Wallaroo Group (Cowley *et al.*, 2003; Fanning *et al.*, 2007). Magmatism of this age occurs elsewhere in the Gawler Craton including the

Tidnamurkana Volcanics of the Peake and Denison inliers in the northern Gawler Craton (Fanning *et al.*, 2007) and unnamed igneous rocks elsewhere in the northwestern Gawler Craton (Howard *et al.*, 2011). That *ca* 1770 Ma magmatic rocks occur beneath the *ca* 1850 Ma Donington Suite is conceivable, and the partial entrainment of some felsic magmatic component of a deeper magmatic rock is possible. Mafic dykes are known to entrain portions of the crust through which they ascend, a spectacular example being lamprophyres of the Grenville Province (Morin *et al.*, 2005). In the case of the mafic dykes of the Southern Yorke
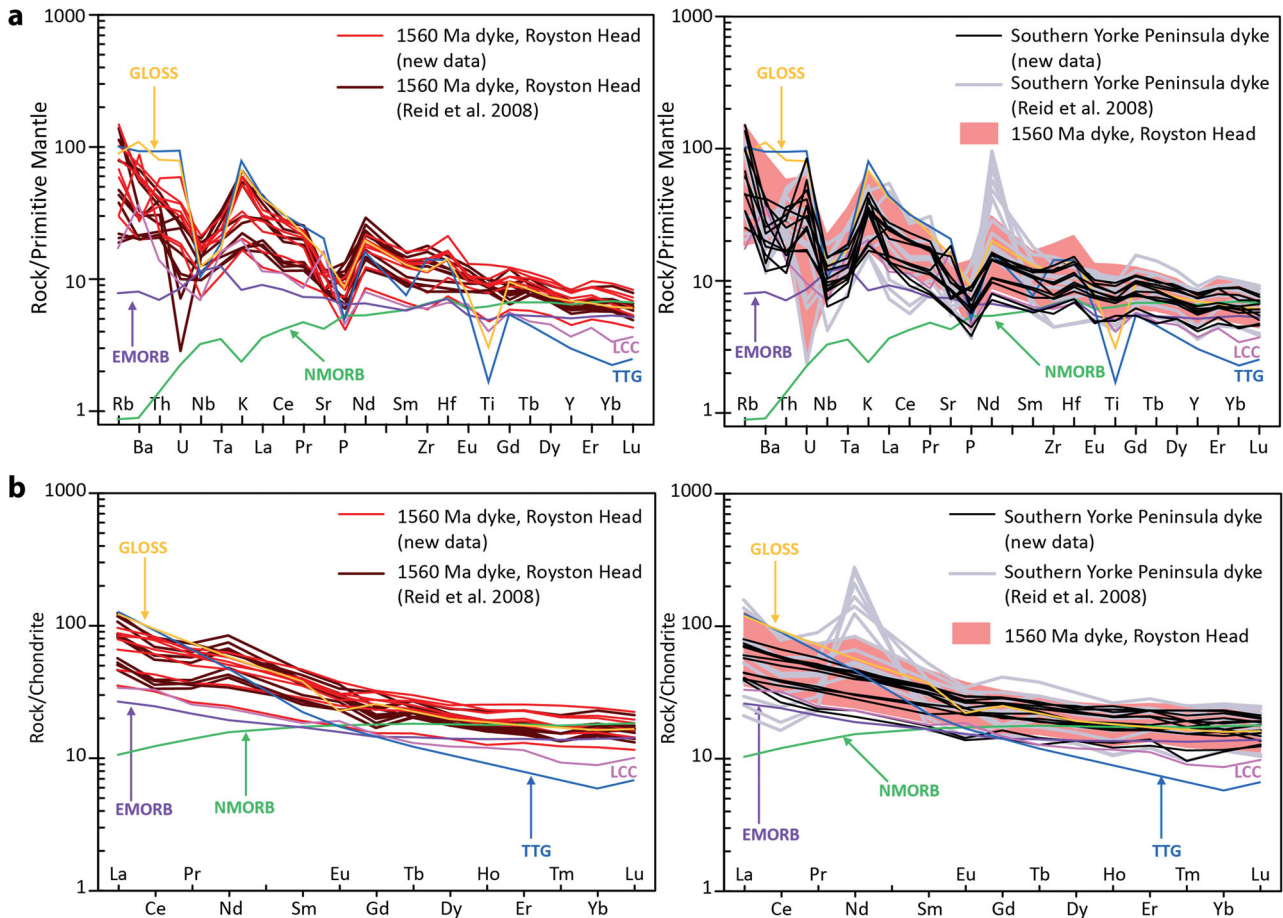
Figure 10. Trace and rare earth element (REE) plots for Daly Head Metadolerite, subdivided into the Royston Head mafic dykes and Southern Yorke Peninsula mafic dykes, shown with respect to normal mid-ocean ridge basalt (NMORB), enriched MORB (EMORB), bulk crust (BC) and global subducting sediment (GLOSS). Normalising values after McDonough and Sun (1995). (a) Primitive mantle-normalised trace element plots for Royston Head mafic dykes (left) and Southern Yorke Peninsula mafic dykes (right) where the shaded pink filed corresponds to trace element data from the Royston Head mafic dykes; and (b) chondrite-normalised REE plots for Royston Head mafic dykes (left) and Southern Yorke Peninsula mafic dykes (right) where the shaded pink filed corresponds to the Royston Head gabbro REE data. Primitive mantle trace element normalising values from Sun and McDonough (1989) and chondrite REE normalising values from McDonough and Sun (1995). Data sources for reservoirs: NMORB: Klein (2004); EMORB: Klein (2004); BC: Rudnick and Gao (2003); GLOSS: Plank and Langmuir (1998).

Table 2. Whole-rock Sm–Nd isotopic data from Daly Head Metadolerite, Southern Yorke Peninsula.

Sample	Age (t)	Nd (ppm)	Sm (ppm)	$^{143}Nd/^{144}Nd$	2σ	$^{147}Sm/^{144}Nd$	$T_{(DM)}$	ε_{Nd} (t)	$\varepsilon_{Nd(0)}$
1893811	1.56 Ga	21.52	5.45	0.512000	0.000002	0.1530	2.9	−3.8	−12.4
1893812	1.56 Ga	25.79	5.85	0.511881	0.000002	0.1371	2.5	−2.9	−14.8
1893813	1.56 Ga	28.98	7.14	0.511988	0.000002	0.1490	2.7	−3.2	−12.7
1893817	1.56 Ga	16.39	4.77	0.512079	0.000002	0.1758	4.2	−6.8	−10.9

Errors on $^{143}Nd/^{144}Nd$ measurements are 2σ (mean) and refer to the last significant figure(s).
Measured ε_{Nd} values calculated with present-day CHUR $^{143}Nd/^{144}Nd$ and $^{147}Sm/^{144}Nd$ ratios of 0.512638 and 0.1966.
Depleted mantle Nd model ages calculated as in Goldstein et al. (1984).

Peninsula, the zircon data reveal the presence of *ca* 1770 Ma magmatic intrusive rocks beneath the Donington Suite.

Geochemical and isotopic constraints on mafic magmatism

Mafic dykes at the Royston Head locality display geochemical affinities with mafic dykes from elsewhere on the Southern Yorke Peninsula, which suggest they can be grouped into a single unit, the Daly Head Metadolerite.

The geochemical data show that the Daly Head Metadolerite is low to moderate in MgO, Mg#, Ni and Cr, suggesting the parent magmas had undergone some degree of crystal fractionation and therefore do not represent primary magma compositions. Trace-element and REE patterns have some features similar to crustal patterns, including negative Nb–Ta and P anomalies, positive K anomalies and similar LREE abundances, but differ in their Ti abundances (Figure 10). Features such as depletions in high-field-strength elements (*e.g.* Nb–Ta–Ti depletions) relative to LILE and LREE and negative ε_{Nd} are commonly associated with the continental crust (Rudnick & Gao, 2003) but
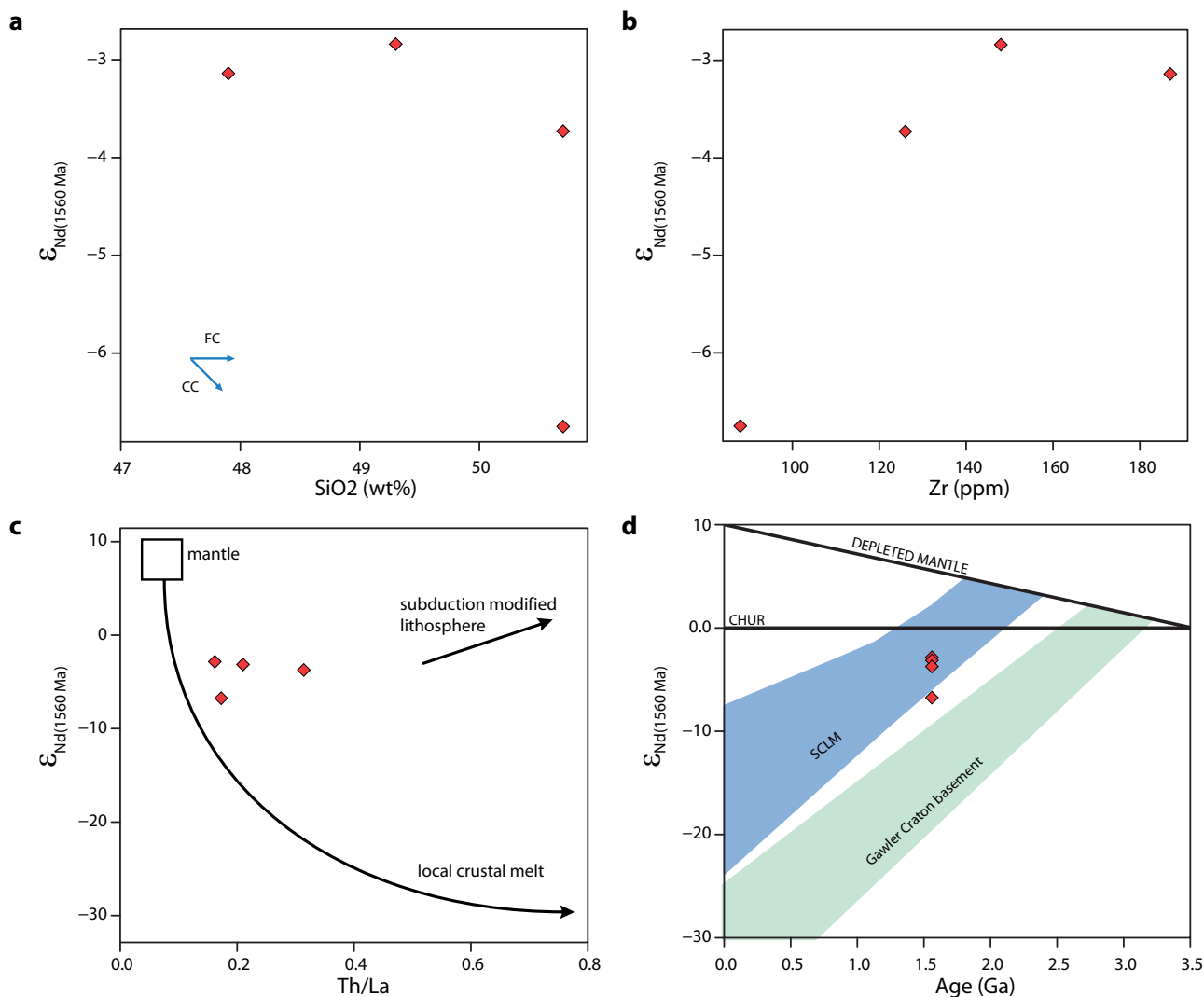
Figure 11. $\varepsilon_{Nd(1560\,Ma)}$ *vs* (a) SiO_2, (b) Zr and (c) Th/La, and (d) Nd isotope evolution for Daly Head Metadolerite. Samples all from the Royston Head locality. Average Archean to Paleoproterozoic Gawler Craton basement (Fraser *et al.*, 2010; Schaefer, 1998; Swain *et al.*, 2005) and subcontinental lithospheric mantle (SCLM) composition based on data from Wade *et al.* (2019) are displayed for comparison.

may also be a feature of convergent margin magmatism (*e.g.* Eiler *et al.*, 1998; Foley *et al.*, 2002; Pearce & Peate, 1995; Prouteau *et al.*, 2001; Stolz *et al.*, 1996). Arguably, the close resemblance of trace element and rare earth element profiles to crustal patterns may be used as evidence for crustal contamination in the Daly Head Metadolerite. However, the absence of a significant negative Ti anomaly and lack of correlation between $\varepsilon_{Nd(1560\,Ma)}$ and SiO_2, Th/La, Zr or MgO does not support large degrees of crustal contamination (Figure 11). Dichotomy between Nd isotopic compositions and MgO, Cr and Zr is also observed in some examples of the Daly Head Metadolerite, primarily those from the Royston Head location, where the low $\varepsilon_{Nd(1560\,Ma)}$ sample has the highest MgO and Cr contents and lowest Zr and Th, and the high $\varepsilon_{Nd(1560\,Ma)}$ samples have low MgO and Cr contents (Figure 11). In the event of crustal contamination, low $\varepsilon_{Nd(1560\,Ma)}$ should be coupled with low MgO and Cr, and high Th and Zr. As this relationship is not observed in some samples, it appears that crustal contamination was variable within the Daly Head Metadolerite,

although we recognise this is a small sample pool. The presence of inherited zircon in the dated sample attests to some degree of crustal contamination in the Daly Head Metadolerite. Nevertheless, crustal contamination does not appear to have been great, with variation in the chemistry likely the result of local controls on magma composition such as crustal residence time for individual magma batches or entrainment of wall rocks in these narrow dykes.

The Daly Head Metadolerite represents tholeiitic gabbros formed in an intraplate, continental to back arc setting (Figure 12a). Enriched lithospheric trace elements such as high Ba, Pb and La are common in continental flood basalts, which reflect a contribution from the continental lithosphere (Baker *et al.*, 2000). Low to moderate combined Nb/La–La/Yb ratios suggest the source region for Daly Head Metadolerite is a mixed asthenospheric–lithospheric mantle source (Figure 12b). The trend in the data on Figure 12b suggests a mixing array with tonalite–trondhjemite–granodiorite (TTG) or GLOSS in the lithospheric
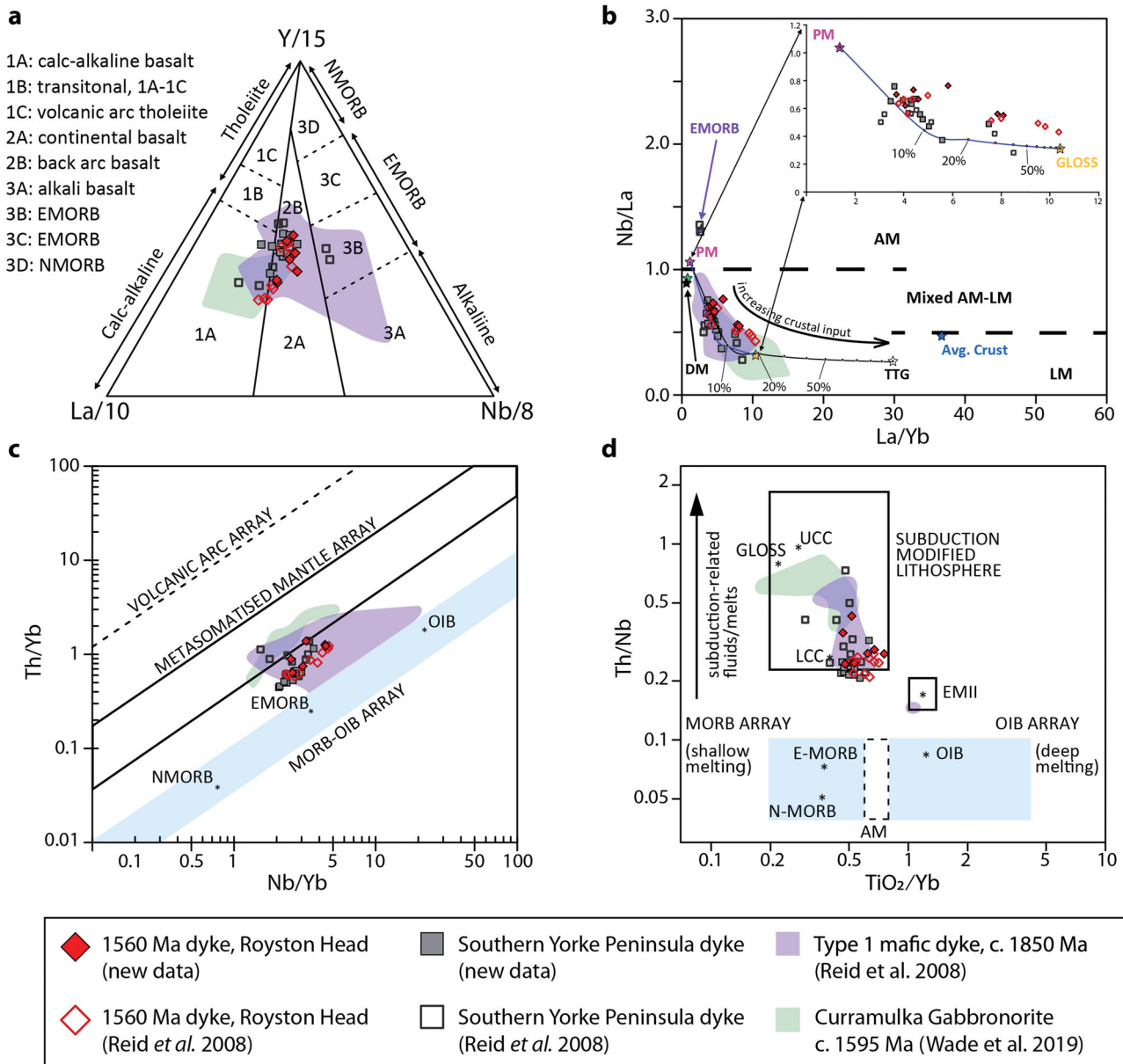
Figure 12. Source region discrimination diagrams for Daly Head Metadolerite, subdivided into the Royston Head mafic dykes and Southern Yorke Peninsula mafic dykes. Also displayed are the fields for mafic rocks that are co-magmatic with the Donington Suite, the so-called 'Type 1' mafic dykes of Reid et al. (2008), and ca 1590 Ma Curramulka Gabbronorite (part of the Hiltaba Suite) from Yorke Peninsula (data from Wade et al., 2019). (a) La–Y–Nb tectonic setting diagram modified from Cabanis and Lecolle (1989); (b) Nb/La vs La/Yb diagram after Abdel-Rahman (2002) showing the mixed asthenospheric mantle (AM) and lithospheric mantle (LM) source region for the Royston Head and other Yorke Peninsula mafic dykes; (c) Th/Yb vs Nb/Yb plot of Pearce (2008); and (d) Th/Nb vs TiO$_2$/Yb plot of Pearce et al. (2015), highlighting the mantle source region for Royston Head mafic dykes and Southern Yorke Peninsula mafic dykes. E-MORB, enriched mid-ocean ridge basalt; N-MORB, normal mid-ocean ridge basalt; OIB, oceanic island basalt; AM, asthenospheric mantle; EMII, enriched mantle 2; LCC, lower continental crust; UCC, upper continental crust; GLOSS, global subducting sediment.

mantle source. The overall SiO$_2$ content of the Daly Head Metadolerite is relatively low, negative anomalies of Nb and Ta are modest and negative Ti anomalies are insignificant, suggesting the degree of crustal assimilation must be proportionally small, and therefore the geochemical enrichment could have been present within the mantle source prior to melt extraction.

Crustal signatures in the lithospheric mantle can result from processes such as crustal contamination or subduction and metasomatism owing to the interaction with melts

and/or fluids and varying degrees of partial melt extraction (Beyer et al., 2006; Farmer et al., 2020; Ionov et al., 2002; O'Reilly & Griffin, 2013). As noted above, crustal contamination in the Daly Head Metadolerite was minimal. Therefore, the enriched signatures in the Daly Head Metadolerite are likely characteristic of an enriched lithospheric mantle source. Elevated Th and Nb relative to Yb place the Daly Head Metadolerite in the metasomatised mantle array and transitional to the MORB-OIB array (Figure 12c). The high Th/Nb ratios correspond to a subduction
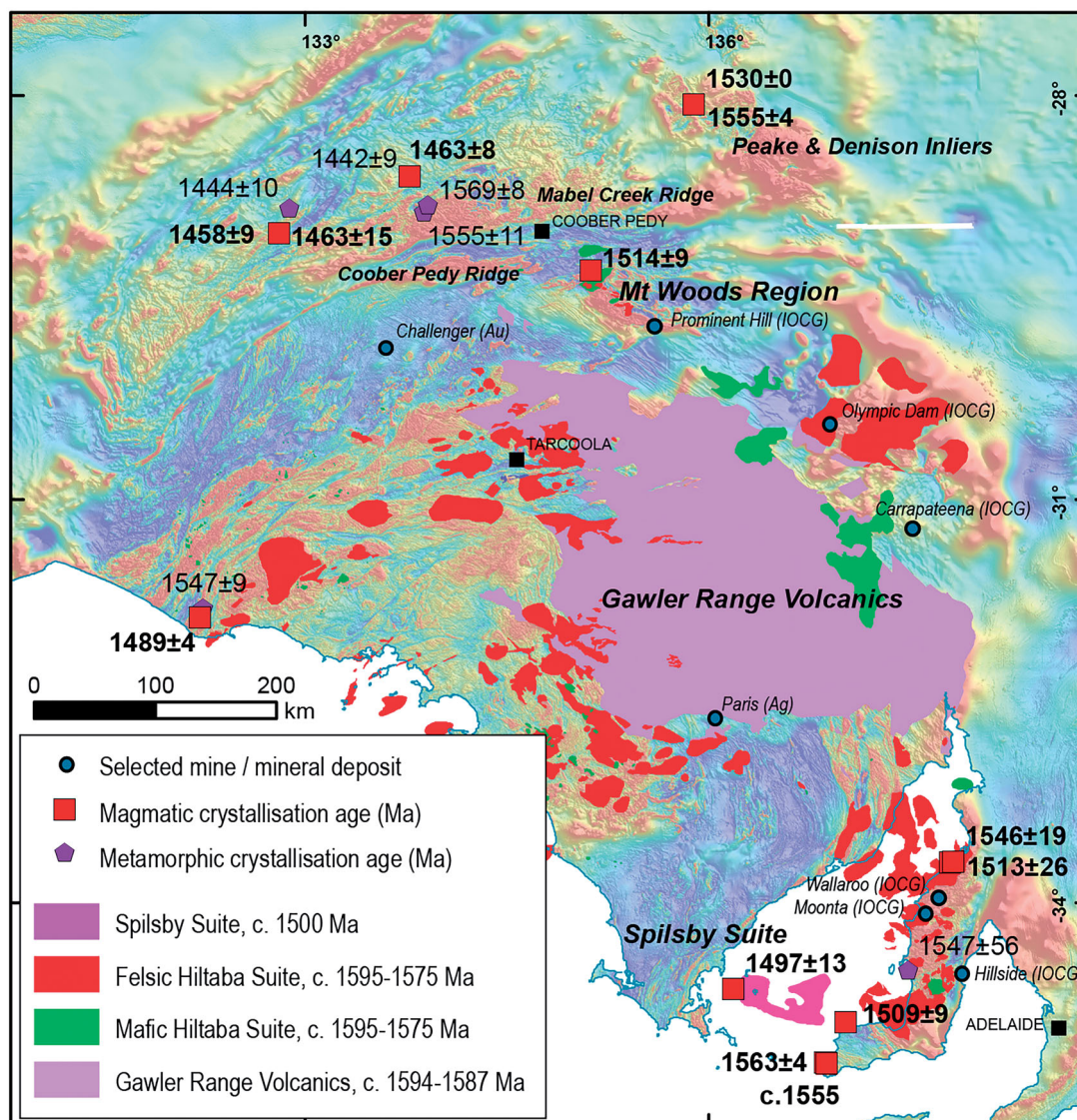
Figure 13. Location of post-1575 Ma magmatic and metamorphic samples from across the Gawler Craton. Individual sample dates are shown, along with the interpreted location of Gawler Range Volcanics and Hiltaba Suite magmatic rocks across the Gawler Craton. Data sources: Fanning *et al.*, 2007; Jagodzinski *et al.*, 2006; Jagodzinski & Reid, 2015; Morrissey *et al.*, 2019; Payne *et al.*, 2008; Reid *et al.*, 2020.

modified lithosphere on Figure 12d, suggesting the enriched compositions of the Daly Head Metadolerite are the result of subduction-related metasomatism in the lithospheric mantle.

Crustal signatures in the lithospheric mantle can result from processes such as subduction and metasomatism owing to interaction with melts and/or fluids and varying degrees of partial melt. Incompatible trace elements such as Th, Nb, Ta and La are sensitive to fluid mobilisation during subduction. As Th is more incompatible than Nb and La during arc metasomatism, the mantle metasomatic process results in an increase in Th/Nb and Th/La ratios (Plank, 2005). Th/La ratios increase to higher ratios where little change is observed in $\varepsilon_{Nd(1560\,Ma)}$, which is more indicative of Th increase relative La owing to metasomatic processes as opposed to crustal contamination (Figure 11c). The Daly

Head Metadolerite is enriched in Th relative to Nb, which is consistent with a metasomatised mantle array transitional to MORB-OIB array (Figure 12c) and subduction modified lithosphere (Figure 12d). The trace-element and isotopic signatures of the Daly Head Metadolerite are therefore likely derived from a metasomatised subduction modified lithosphere. Low to moderate TiO_2/Yb ratios are consistent with shallow melting, and together with the lack of Eu anomaly and the moderate HREE compositions, melting likely occurred in the plagioclase rather than garnet stability field. This is also supported by unfractionated HREE, which also is indicative of derivation from above the garnet stability field from within the lithospheric mantle.

Existence of an enriched lithospheric mantle beneath the Gawler Craton has been suggested by a number of previous studies (Huang *et al.*, 2016; Skirrow *et al.*, 2018;

Wade et al., 2019). The metasomatised and enriched sub-continental lithospheric mantle (SCLM) beneath the Gawler Craton is recognised as an ancient element, likely to have been formed during the Archean (Reid et al., 2009; Skirrow et al., 2018; Swain et al., 2005; Wade et al., 2019). The SCLM as defined by Wade et al. (2019) is isotopically indistinguishable from the source of the Daly Head Metadolerite (Figure 11d). The negative $\varepsilon_{Nd(1560\,Ma)}$ values and Archean to Paleoproterozoic T_{DM} model ages support derivation of the mafic dykes from an ancient lithospheric mantle source, which may be similar to the SCLM that was partially melted during formation of the ca 1595–1575 Ma Gawler Range Volcanics and Hiltaba Suite magmatic event.

Timing and significance of late-stage shear zone development and granite emplacement: extent of the early Mesoproterozoic magmatism and metamorphism in the Southern Yorke Peninsula

The basement exposures at Royston Head show that the Donington Suite orthogneiss and the ca 1564 Ma mafic dykes of the Daly Head Metadolerite were locally reworked by narrow high-strain zones. Within one example of these high-strain zones, a syn-kinematic granitic dyke has been dated at ca 1555 Ma. Previously, these high-strain zones were interpreted to be part of a late stage of the ca 1850 Ma Cornian Orogeny (Reid et al., 2008); however, it now appears this interpretation is incorrect, and these high-strain zones can be ascribed to a period of early Mesoproterozoic deformation. The regional extent of this deformation is unknown at present. It may be that other high-strain zones within the Donington Suite are also of a similar age. The new data also raise the possibility that other deformation fabrics in the southeastern Gawler Craton could also post-date the Hiltaba Suite magmatic event and could be part of a younger event.

Implications for the regional tectonics of the Gawler Craton

The major tectono-magmatic event of Gawler Craton during the early Mesoproterozoic occurred over the interval ca 1596–1575 Ma (Daly et al., 1998; Forbes et al., 2011; Hand et al., 2007; Tiddy et al., 2020). Tectonic activity did not cease in the Gawler Craton subsequent to this time. In fact, increasing evidence suggests medium- to high-temperature processes continued for the next 50–100 my (Figure 13), and these include:

- the Spilsby Suite, a localised series of granitic plutons emplaced at ca 1510 Ma in the southern Gawler Craton (Fanning et al., 2007; Rankin et al., 2006; Reid, Zhao, et al., 2020);
- metamorphism of metabasic units of the Wallaroo Group at 1547 ± 56 Ma (Renowden Metabasalt Member; Reid, Zhao, et al., 2020);

- metamorphic zircon growth at 1566 ± 9 Ma in the Coober Pedy Ridge of the northern Gawler Craton (Hand et al., 2007);
- metamorphic zircon growth at ca 1510 Ma in the Mabel Creek Ridge of the northern Gawler Craton (Reid et al., 2014);
- granitic magmatism at 1555 ± 14 Ma in the Peake and Denison inliers, northern Gawler Craton (Fanning et al., 2007);
- granitic magmatism at ca 1450 Ma in the northern Gawler Craton associated with crustal reworking, which was widespread across the northern and western Gawler Craton between ca 1480 and 1410 Ma (Fraser et al., 2012; Fraser & Lyons, 2006; Morrissey et al., 2019; Reid & Forster, 2021); and
- pegmatite intrusion into gneisses of the Fowler Domain, western Gawler Craton at ca 1490 Ma (Fanning et al., 2007).

These magmatic and/or deformation events appear to have occurred at the periphery of the Gawler Craton, in regions away from where Gawler Range Volcanics and Hiltaba Suite magmatism is the most widespread (Figure 13). A possible explanation for this spatial localisation of magmatism is that the central Gawler Craton lithosphere was less fertile for formation of younger magmatic phases.

The Gawler Range Volcanics and Hiltaba Suite were derived from high-temperature magmas, with some Gawler Range Volcanics units containing inverted pigeonite phenocrysts suggesting magmatic temperatures of 950–1100 °C (Allen et al., 2008; Pankhurst et al., 2011). Pankhurst et al. (2013) suggested that high-temperature magmatism such as the Gawler Range Volcanics and associated Hiltaba Suite can result in stabilisation of the lithospheric column as a consequence of the intensive fusion of the heterogeneous lower crust and upper mantle. The redistribution of heat-producing elements (U, Th and K) into the upper crust also modifies the lithospheric thermal profile and therefore melting potential (McLaren et al., 2003). A consequence is that the remaining lower crust and upper mantle become dominated by restite compositions, which are relatively infertile during subsequent thermal events. Nevertheless, the ca 1564 Ma mafic magmatism in the Southern Yorke Peninsula manifest as the Daly Head Metadolerite was derived from a metasomatised mantle source region. This could be hinting that the mantle source region in this portion of the Gawler Craton escaped widespread fusion during the Gawler Range Volcanics–Hiltaba Suite magmatic event, as is inferred for the central portions of the Gawler Craton. If this were the case, the mantle in the southeastern Gawler Craton may have retained some of the prior metasomatic composition, leaving it fertile for a melting event subsequent to Hiltaba Suite magmatism.

Finally, we note that Hand et al. (2007) considered the ca 1570–1540 Ma events in the Gawler Craton to be part of the Kararan Orogeny; however, nomenclatures for

describing the tectonic and magmatic events of this time period are not well established (Fraser *et al.*, 2012). Further work on the Yorke Peninsula and elsewhere in the Gawler Craton will enable mapping of the extent of tectonic activity post *ca* 1570 Ma and will help unravel the nature of the reworking that the Gawler Craton underwent at this time.

Conclusions

Geochronological data from zircon within a planar mafic dyke on Southern Yorke Peninsula demonstrate a mafic magmatic event in the region at *ca* 1564 Ma that formed a series of mafic dykes we term the Daly Head Metadolerite. Previous interpretation that these mafic dykes formed during the late stages of the *ca* 1845 Ma Cornian Orogeny (Reid *et al.*, 2008) was based on field relationships alone and can be now considered incorrect. Daly Head Metadolerite samples have elevated LILE and LREE together with negative $\varepsilon_{Nd(1560\,Ma)}$ values, suggesting that these mafic dykes were derived from a continental lithospheric source that was potentially enriched as part of an ancient subduction regime. Localised deformation post-dates the emplacement of these mafic dykes, with a syn-kinematic granitic sheet having been emplaced at *ca* 1555 Ma. These new data are the first evidence for an early Mesoproterozoic deformation event in this region that post-dates the voluminous and metallogenically significant Gawler Range Volcanics and Hiltaba Suite magmatism. Further work is needed to clarify the extent of this younger event and to correlate it with other events across the region.

Acknowledgements

Disclosure statement

Funding

ORCID

A. J. Reid 🔾 http://orcid.org/0000-0002-9435-9342
C. E. Wade 🔾 http://orcid.org/0000-0003-2569-2771
E. A. Jagodzinski 🔾 http://orcid.org/0000-0002-0151-2337

Data availability statement

References

Abdel-Rahman, A-F. M. (2002). Mesozoic volcanism in the Middle East: geochemical, isotopic and petrogenetic evolution of extension-related alkali basalts from central Lebanon. *Geological Magazine*, *139*(6), 621–640. https://doi.org/10.1017/S0016756802006829

Aitken, A. R. A., Betts, P. G., Young, D. A., Blankenship, D. D., Roberts, J. L., & Siegert, M. J. (2016). The Australo-Antarctic Columbia to Gondwana transition. *Gondwana Research*, *29*(1), 136–152. https://doi.org/10.1016/j.gr.2014.10.019

Allen, S. R., McPhie, J., Ferris, G., & Simpson, C. (2008). Evolution and architecture of a large felsic igneous province in western Laurentia: The 1.6 Ga Gawler Range Volcanics, South Australia. *Journal of Volcanology and Geothermal Research*, *172*(1–2), 132–147. https://doi.org/10.1016/j.jvolgeores.2005.09.027

Baker, J. A., MacPherson, C. G., Menzies, M. A., Thirlwall, M. F., Al-Kadasi, M., & Mattey, D. P. (2000). Resolving crustal and mantle contributions to continental flood volcanism, Yemen; constraints from mineral oxygen isotope data. *Journal of Petrology*, *41*(12), 1805–1820. https://doi.org/10.1093/petrology/41.12.1805

Betts, P. G., Armit, R. J., Stewart, J., Aitken, A. R. A., Ailleres, L., Donchak, P., Hutton, L., Withnall, I., & Giles, D. (2016). Australia and Nuna. *Geological Society, London, Special Publications*, *424*(1), 47–81. https://doi.org/10.1144/SP424.2

Beyer, E. E., Griffin, W. L., & O'Reilly, S. Y. (2006). Transformation of Archaean lithospheric mantle by refertilization: Evidence from exposed peridotites in the Western Gneiss Region, Norway. *Journal of Petrology*, *47*(8), 1611–1636. https://doi.org/10.1093/petrology/egl022

Bhattacharya, S., Kemp, A. I. S., & Collins, W. J. (2018). Response of zircon to melting and metamorphism in deep arc crust, Fiordland (New Zealand): Implications for zircon inheritance in Cordilleran granites. *Contributions to Mineralogy and Petrology*, *173*(4), 28. https://doi.org/10.1007/s00410-018-1446-5

Black, L. P., Kamo, S. L., Williams, I. S., Mundil, R., Davis, D. W., Korsch, R. J., & Foudoulis, C. (2003). The application of SHRIMP to Phanerozoic geochronology; a critical appraisal of four zircon standards. *Chemical Geology*, *200*(1–2), 171–188. https://doi.org/10.1016/S0009-2541(03)00166-9

Black, L. P., Kamo, S. L., Allen, C. M., Davis, D. W., Aleinikoff, J. N., Valley, J. W., Mundil, R., Campbell, I. H., Korsch, R. J., Williams, I. S., & Foudoulis, C. (2004). Improved $^{206}Pb/^{238}U$ microprobe geochronology by the monitoring of a trace-element-related matrix effect; SHRIMP, ID-TIMS, ELA-ICP-MS and oxygen isotope documentation for a series of zircon standards. *Chemical Geology*, *205*(1–2), 115–140. https://doi.org/10.1016/j.chemgeo.2004.01.003

Blissett, A. H., Creaser, R. A., Daly, S., Flint, D. J., & Parker, A. J. (1993). Gawler Range Volcanics. In J. F. Drexel, W. V. Preiss, & A. J. Parker (Eds.), *The geology of South Australia. Vol 1. The Precambrian* (pp. 107–131). Geological Survey of South Australia. Bulletin 54.

Brotodewo, A., Tiddy, C. J., Reid, A., Wade, C., & Conor, C. (2018). Relationships between magmatism and deformation in northern Yorke Peninsula and southeastern Proterozoic Australia. *Australian*

Journal of Earth Sciences, 65(5), 619–641. https://doi.org/10.1080/08120099.2018.1470573

Budd, A. (2006). *The Tarcoola Goldfield of the Central Gawler Gold Province, and the Hiltaba Association Granites, Gawler Craton* [South Australia PhD thesis]. Australian National University.

Budd, A. R., & Fraser, G. L. (2004). Geological relationships and $^{40}Ar/^{39}Ar$ age constraints on gold mineralisation at Tarcoola, central Gawler gold province, South Australia. *Australian Journal of Earth Sciences*, 51(5), 685–700. https://doi.org/10.1111/j.1400-0952.2004.01084.x

Cabanis, B., & Lecolle, M. (1989). Le diagramme La/10–Y/15–Nb/8: Un outil pour la discrimination des series volcaniques et lamise en evidence des processus demelange et/ou de contamination crustale. *Compte Rendus de l'Académie des Sciences Series II*, 309, 2023–2029.

Conor, C. (1995). *Moonta-Wallaroo region: An interpretation of the geology of the Maitland and Wallaroo 1:100 000 sheet areas* (Vol. Open file Envelope, 8886). South Australia. Department of Primary Industries and Resources.

Conor, C. C. H., Raymond, O., Baker, T., Teale, G. S., Say, P., & Lowe, G. (2010). Alteration and mineralisation in the Moonta-Wallaroo copper–gold mining field region, Olympic Domain, South Australia. In T. M. Porter (Ed.), *Hydrothermal iron oxide copper–gold & related deposits: A global perspective, v. 3—advances in the understanding of IOCG deposits* (pp. 1–24). PGC Publishing.

Courtney-Davies, L., Ciobanu, C. L., Tapster, S. R., Cook, N. J., Ehrig, K., Crowley, J. L., Verdugo-Ihl, M. R., Wade, B. P., & Condon, D. J. (2020). Opening the magmatic-hydrothermal window: high-precision U–Pb geochronology of the Mesoproterozoic Olympic Dam Cu–Au–U–Ag deposit. *Economic Geology*, 115(8), 1855–1870. https://doi.org/10.5382/econgeo.4772

Cowley, W. M., Conor, C. H. H., & Zang, W. (2003). New and revised Proterozoic stratigraphic units on northern Yorke Peninsula. *MESA Journal*, 29, 46–58.

Daly, S. J., Fanning, C. M., & Fairclough, M. C. (1998). Tectonic evolution and exploration potential of the Gawler Craton, South Australia. *AGSO Journal of Australian Geology & Geophysics*, 17, 145–168.

Ehrig, K., McPhie, J., & Kamenetsky, V. (2012). Geology and mineralogical zonation of the Olympic Dam iron oxide Cu–U–Au–Ag deposit, South Australia. In J. W. Hedenquist, M. Harris, & F. Camus (Eds.), *Geology and genesis of major copper deposits and districts of the world: A tribute to Richard H. Sillitoe* (pp. 237–267). Society of Economic Geologists Special Publication 16.

Eiler, J. M., McInnes, B., Valley, J. W., Graham, C. M., & Stolper, E. M. (1998). Oxygen isotope evidence for slab-derived fluids in the subarc mantle. *Nature*, 393(6687), 777–781. https://doi.org/10.1038/31679

Fanning, C. M., Flint, R. B., & Preiss, W. V. (1983). Geochronology of the Pandurra Formation. *Quarterly Geological Notes—Geological Survey of South Australia*, 88, 11–16.

Fanning, C. M., Reid, A. J., Teale, G. (2007). *A geochronological framework for the Gawler Craton, South Australia*. South Australia Geological Survey. Bulletin 55. https://sarigbasis.pir.sa.gov.au/WebtopEw/ws/samref/sarig1/image/DDD/BULL055.pdf

Farina, F., Stevens, G., Gerdes, A., & Frei, D. (2014). Small-scale Hf isotopic variability in the Peninsula pluton (South Africa): The processes that control inheritance of source $^{176}Hf/^{177}Hf$ diversity in S-type granites. *Contributions to Mineralogy and Petrology*, 168(4), 1065. https://doi.org/10.1007/s00410-014-1065-8

Farmer, G. L., Fritz, D. E., & Glazner, A. F. (2020). Identifying metasomatized continental lithospheric mantle involvement in Cenozoic magmatism from Ta/Th values, southwestern North America. *Geochemistry, Geophysics, Geosystems*, 21(5), e2019GC008499. https://doi.org/10.1029/2019GC008499

Flint, R. B., Blissett, A. H., Conor, C. H. H., Cowley, W. M., Cross, K. C., Creaser, R. A., Daly, S. J., Krieg, G. W., Major, R. B., Teale, G. S., & Parker, A. J. (1993). Mesoproterozoic. In J. F. Drexel, W. V. Preiss, & A. J. Parker (Eds.), *The geology of South Australia; Volume 1, The Precambrian* (pp. 106–169). Geological Survey of South Australia. Bulletin 54.

Flint, R. B., Rankin, L. R., & Fanning, C. M. (1990). Definition; the Palaeoproterozoic St. Peter Suite of the western Gawler Craton. *Quarterly Geological Notes—Geological Survey of South Australia*, 114, 2–8.

Foley, S., Tiepolo, M., & Vannucci, R. (2002). Growth of early continental crust controlled by melting of amphibolite in subduction zones. *Nature*, 417(6891), 837–840. https://doi.org/10.1038/nature00799

Forbes, C. J., Giles, D., Hand, M., Betts, P. G., Suzuki, K., Chalmers, N. C., & Dutch, R. (2011). Using P–T paths to interpret the tectonothermal setting of prograde metamorphism: An example from the northeastern Gawler Craton, South Australia. *Precambrian Research*, 185(1–2), 65–85. https://doi.org/10.1016/j.precamres.2010.12.002

Fraser, G., & Lyons, P. (2006). Timing of Mesoproterozoic tectonic activity in the northwestern Gawler Craton constrained by $^{40}Ar/^{39}Ar$ geochronology. *Precambrian Research*, 151(3–4), 160–184. https://doi.org/10.1016/j.precamres.2006.08.007

Fraser, G., McAvaney, S., Neumann, N., Szpunar, M., & Reid, A. (2010). Discovery of early Mesoarchean crust in the eastern Gawler Craton, South Australia. *Precambrian Research*, 179(1–4), 1–21. https://doi.org/10.1016/j.precamres.2010.02.008

Fraser, G., Reid, A., & Stern, R. (2012). Timing of deformation and exhumation across the Karari Shear Zone, north-western Gawler Craton, South Australia. *Australian Journal of Earth Sciences*, 59(4), 547–570. https://doi.org/10.1080/08120099.2012.678586

Fraser, G. L., Bagas, L., & Huston, D. L. (2012). $^{40}Ar/^{39}Ar$ evidence for the timing of Paleoproterozoic gold mineralisation at the Sandpiper Deposit, Tanami region, northern Australia. *Australian Journal of Earth Sciences*, 59(3), 399–409. https://doi.org/10.1080/08120099.2012.656325

Giles, D., Betts, P. G., & Lister, G. S. (2004). 1.8–1.5-Ga links between the North and South Australian Cratons and the Early–Middle Proterozoic configuration of Australia. *Tectonophysics*, 380(1–2), 27–41. https://doi.org/10.1016/j.tecto.2003.11.010

Goldstein, S. L., Onions, R. K., & Hamilton, P. J. (1984). A Sm–Nd isotopic study of atmospheric dusts and particulates from major river systems. *Earth and Planetary Science Letters*, 70(2), 221–236. https://doi.org/10.1016/0012-821x(84)90007-4

Griffin, W. L., Powell, W. J., Pearson, N. J., & O'Reilly, S. Y. (2008). GLITTER: data reduction software for laser ablation ICP-MS, Laser Ablation-ICP-MS in the Earth Sciences. *Mineralogical Association of Canada Short Course Series*, 40, 204–207.

Hand, M., Reid, A., & Jagodzinski, E. (2007). Tectonic framework and evolution of the Gawler Craton, South Australia. *Economic Geology*, 102(8), 1377–1395. https://doi.org/10.2113/gsecongeo.102.8.1377

Hoek, J. D., & Schaefer, B. F. (1998). Palaeoproterozoic Kimban mobile belt, Eyre Peninsula; timing and significance of felsic and mafic magmatism and deformation. *Australian Journal of Earth Sciences*, 45(2), 305–313. https://doi.org/10.1080/08120099808728389

Hoskin, P. W. O., & Schaltegger, U. (2003). The composition of zircon and igneous and metamorphic petrogenesis. *Reviews in Mineralogy and Geochemistry*, 53(1), 27–62. https://doi.org/10.2113/0530027

Howard, K. E., Hand, M., Barovich, K. M., Payne, J. L., Cutts, K. A., & Belousova, E. A. (2011). U–Pb zircon, zircon Hf and whole-rock Sm–Nd isotopic constraints on the evolution of Paleoproterozoic rocks in the northern Gawler Craton. *Australian Journal of Earth Sciences*, 58(6), 615–638. https://doi.org/10.1080/08120099.2011.594905

Huang, Q., Kamenetsky, V. S., Ehrig, K., McPhie, J., Kamenetsky, M., Cross, K., Meffre, S., Agangi, A., Chambefort, I., Direen, N. G., Maas, R., & Apukhtina, O. (2016). Olivine-phyric basalt in the Mesoproterozoic Gawler silicic large igneous province, South Australia: Examples at the Olympic Dam Iron Oxide Cu–U–Au–Ag deposit and other localities. *Precambrian Research*, 281, 185–199. https://doi.org/10.1016/j.precamres.2016.05.019

Huang, Q., Kamenetsky, V. S., McPhie, J., Ehrig, K., Meffre, S., Maas, R., Thompson, J., Kamenetsky, M., Chambefort, I., Apukhtina, O., & Hu,

Y. (2015). Neoproterozoic (ca. 820–830 Ma) mafic dykes at Olympic Dam, South Australia: Links with the Gairdner Large Igneous Province. *Precambrian Research*, *271*, 160–172. https://doi.org/10.1016/j.precamres.2015.10.001

Ionov, D. A., Bodinier, J-L., Mukasa, S. B., & Zanetti, A. (2002). Mechanisms and sources of mantle metasomatism: major and trace element compositions of peridotite xenoliths from Spitsbergen in the context of numerical modelling. *Journal of Petrology*, *43*(12), 2219–2259. https://doi.org/10.1093/petrology/43.12.2219

Irvine, T. N., & Baragar, W. R. A. (1971). A guide to the chemical classification of the common volcanic rocks. *Canadian Journal of Earth Sciences*, *8*(5), 523–548. https://doi.org/10.1139/e71-055

Jackson, S. E., Pearson, N. J., Griffin, W. L., & Belousova, E. A. (2004). The application of laser ablation-inductively coupled plasma-mass spectrometry to in situ U–Pb zircon geochronology. *Chemical Geology*, *211*(1–2), 47–69. https://doi.org/10.1016/j.chemgeo.2004.06.017

Jagodzinski, E. A., Black, L., Frew, R. A., Foudoulis, C., Reid, A., Payne, J., Zang, W., & Schwarz, M. P. (2006). *Compilation of SHRIMP U–Pb geochronological data for the Gawler Craton, South Australia 2005–2006*. Primary Industries and Resources South Australia Report Book. 2006/20.

Jagodzinski, E. A., & Reid, A. J. (2015). *PACE geochronology: Results of collaborative geochronology projects, 2013–2015*. Government of South Australia. Department of the Premier and Cabinet. Report Book, 2015/00003.

Kirkland, C. L., Smithies, R. H., Taylor, R. J. M., Evans, N., & McDonald, B. (2015). Zircon Th/U ratios in magmatic environs. *Lithos*, *212–215*, 397–414. https://doi.org/10.1016/j.lithos.2014.11.021

Klein, E. M. (2004). Geochemistry of the igneous oceanic crust. In H. D. Holland & K. K. Turekian (Eds.), *Treatise on Geochemistry* (Vol. 3, pp. 433–463). Elsevier.

Lee, C-T A., Luffi, P., Plank, T., Dalton, H., & Leeman, W. P. (2009). Constraints on the depths and temperatures of basaltic magma generation on Earth and other terrestrial planets using new thermobarometers for mafic magmas. *Earth and Planetary Science Letters*, *279*(1–2), 20–33. https://doi.org/10.1016/j.epsl.2008.12.020

Lloyd, J. C., Blades, M. L., Counts, J. W., Collins, A. S., Amos, K. J., Wade, B. P., Hall, J. W., Hore, S., Ball, A. L., Shahin, S., & Drabsch, M. (2020). Neoproterozoic geochronology and provenance of the Adelaide Superbasin. *Precambrian Research*, *350*, 105849. https://doi.org/10.1016/j.precamres.2020.105849

Ludwig, K. R. (2003). *Isoplot 3.00—a geochronological toolkit for Microsoft Excel*. Berkeley Geochronology Center Special Publication No. 4.

Ludwig, K. R. (2009). *SQUID 2.50: A user's manual*. Berkeley Geochronology Center Special Publication. No. 5.

McDonough, W. F., & Sun, S-S. (1995). Composition of the Earth. *Chemical Geology*, *120*(3-4), 223–253. https://doi.org/10.1016/0009-2541(94)00140-4

McLaren, S., Sandiford, M., Hand, M., Neumann, N., Wyborn, L., & Bastrakova, I. (2003). The hot southern continent. Heat flow and heat production in Australian Proterozoic terranes. In R. R. Hillis & D. Muller (Eds.), *Evolution and dynamics of the Australian Plate* (Vol. 22, pp. 151–161). Geological Society of Australia, Special Publication.

Middlemost, E. A. K. (1994). Naming materials in the magma/igneous rock system. *Earth-Science Reviews*, *37*(3-4), 215–224. https://doi.org/10.1016/0012-8252(94)90029-9

Morin, D., Hébert, R., & Corriveau, L. (2005). Mesoproterozoic deep K-magmatism recorded in a megacryst- and xenolith-bearing minette dyke, western Grenville Province. *Canadian Journal of Earth Sciences*, *42*(10), 1881–1906. https://doi.org/10.1139/e05-083

Morrissey, L. J., Barovich, K. M., Hand, M., Howard, K. E., & Payne, J. L. (2019). Magmatism and metamorphism at ca. 1.45 Ga in the northern Gawler Craton: The Australian record of rifting within Nuna (Columbia). *Geoscience Frontiers*, *10*(1), 175–194. https://doi.org/10.1016/j.gsf.2018.07.006

Mortimer, G. E., Cooper, J. A., & Oliver, R. L. (1988). Proterozoic mafic dykes near Port Lincoln, South Austrlia: composition, age and origin. *Australian Journal of Earth Sciences*, *35*(1), 93–110. https://doi.org/10.1080/08120098808729442

O'Reilly, S. Y., & Griffin, W. L. (2013). Mantle metasomatism. In *Metasomatism and the chemical transformation of rock: The role of fluids in terrestrial and extraterrestrial processes* (pp. 471–533). Springer Berlin Heidelberg. https://doi.org/10.1007/978-3-642-28394-9_12

Pankhurst, M. J., Schaefer, B. F., Betts, P. G., Phillips, N., & Hand, M. (2011). A Mesoproterozoic continental flood rhyolite province, the Gawler Ranges, Australia: The end member example of the Large Igneous Province clan. *Solid Earth.*, *2*(1), 25–33. https://doi.org/10.5194/se-2-25-2011

Pankhurst, M. J., Schaefer, B. F., Turner, S. P., Argles, T., & Wade, C. E. (2013). The source of A-type magmas in two contrasting settings: U–Pb, Lu–Hf and Re–Os isotopic constraints. *Chemical Geology*, *351*, 175–194. https://doi.org/10.1016/j.chemgeo.2013.05.010

Parker, A. J., Daly, S. J., Flint, D. J., Flint, R. B., Preiss, W. V., & Teale, G. S. (1993). Palaeoproterozoic. In J. F. Drexel, W. V. Preiss, & A. J. Parker (Eds.), *The geology of South Australia; Volume 1, The Precambrian* (Vol. 1, pp. 50–105). Geological Survey of South Australia. Bulletin 54.

Payne, J., Barovich, K., & Hand, M. (2006). Provenance of metasedimentary rocks in the northern Gawler Craton, Australia: Implications for Palaeoproterozoic reconstructions. *Precambrian Research*, *148*(3–4), 275–291. https://doi.org/10.1016/j.precamres.2006.05.002

Payne, J., Hand, M., Barovich, K., & Wade, B. (2008). Temporal constraints on the timing of high-grade metamorphism in the northern Gawler Craton: Implications for assembly of the Australian Proterozoic. *Australian Journal of Earth Sciences*, *55*(5), 623–640. https://doi.org/10.1080/08120090801982595

Payne, J. L., Ferris, G., Barovich, K. M., & Hand, M. (2010). Pitfalls of classifying ancient magmatic suites with tectonic discrimination diagrams: An example from the Paleoproterozoic Tunkillia Suite, southern Australia. *Precambrian Research*, *177*(3–4), 227–240. https://doi.org/10.1016/j.precamres.2009.12.005

Pearce, J. A. (2008). Geochemical fingerprinting of oceanic basalts with applications to ophiolite classification and the search for Archean oceanic crust. *Lithos*, *100*(1–4), 14–48. https://doi.org/10.1016/j.lithos.2007.06.016

Pearce, J. A., Ernst, R. E., & Peate, D. W. (2015). A geochemical proxy approach to LIP forensics. Abstracts—Geological Association of Canada 38. https://doi.org/10.1130/abs/2017AM-301471

Pearce, J. A., & Peate, D. W. (1995). Tectonic implications of the composition of volcanic arc magmas. *Annual Review of Earth and Planetary Sciences*, *23*(1), 251–285. https://doi.org/10.1146/annurev.ea.23.050195.001343

Plank, T. (2005). Constraints from thorium/lanthanum on sediment recycling at subduction zones and the evolution of the continents. *Journal of Petrology*, *46*(5), 921–944. https://doi.org/10.1093/petrology/egi005

Plank, T., & Langmuir, C. H. (1998). The chemical composition of subducting sediment and its consequences for the crust and mantle. *Chemical Geology*, *145*(3–4), 325–394. https://doi.org/10.1016/S0009-2541(97)00150-2

Prouteau, G., Scaillet, B., Pichavant, M., & Maury, R. (2001). Evidence for mantle metasomatism by hydrous silicic melts derived from subducted oceanic crust. *Nature*, *410*(6825), 197–200. https://doi.org/10.1038/35065583

Rankin, L. R., Fanning, C. M., Flint, R. B., & Chalmers, N. C. (2006). *Proterozoic geology of islands in southern Spencer Gulf, southern Gawler Craton*. Department of Primary Industries and Resources. Report Book, 2006/8.

Reid, A. (2019). The Olympic Cu–Au Province, Gawler Craton: A review of the lithospheric architecture, geodynamic setting, alteration systems, cover successions and prospectivity. *Minerals*, *9*(6), 371. https://doi.org/10.3390/min9060371

Reid, A., & Forster, M. (2021). Mesoproterozoic thermal evolution of the northern Gawler Craton from $^{40}Ar/^{39}Ar$ geochronology.

Precambrian Research, 358, 106180. https://doi.org/10.1016/j.pre-camres.2021.106180

Reid, A. J., & Fabris, A. (2015). Influence of pre-existing low meta-morphic grade sedimentary successions on the distribution of iron oxide copper–gold mneralization in the Olympic Cu–Au Province, Gawler Craton. *Economic Geology, 110*(8), 2147–2157. https://doi.org/10.2113/econgeo.110.8.2147

Reid, A. J., Fricke, C., & Cowley, W. M. (2009). Extent of the low-grade Archaean Devils Playground Volcanics in the north-eastern Gawler Craton: Evidence from recent PACE drilling. *MESA Journal, 54,* 9–19.

Reid, A. J., Hand, M., Jagodzinski, E., Kelsey, D., & Pearson, N. J. (2008). Palaeoproterozoic orogenesis within the southeastern Gawler Craton, South Australia. *Australian Journal of Earth Sciences, 55*(4), 449–471. https://doi.org/10.1080/08120090801888594

Reid, A. J., Jagodzinski, E. A., Armit, R. J., Dutch, R. A., Kirkland, C. L., Betts, P. G., & Schaefer, B. F. (2014). U–Pb and Hf isotopic evidence for Neoarchean and Paleoproterozoic basement in the buried northern Gawler Craton, South Australia. *Precambrian Research, 250*(0), 127–142. https://doi.org/10.1016/j.precamres.2014.05.019

Reid, A. J., Jagodzinski, E. A., Fraser, G. L., & Pawley, M. J. (2014). SHRIMP U–Pb zircon age constraints on the tectonics of the Neoarchean to early Paleoproterozoic transition within the Mulgathing Complex, Gawler Craton, South Australia. *Precambrian Research, 250*(0), 27–49. https://doi.org/10.1016/j.precamres.2014.05.013

Reid, A. J., Pawley, M. J., Wade, C., Jagodzinski, E. A., Dutch, R. A., & Armstrong, R. (2020). Resolving tectonic settings of ancient mag-matic suites using structural, geochemical and isotopic constraints: The example of the St Peter Suite, southern Australia. *Australian Journal of Earth Sciences, 67*(1), 31–58. https://doi.org/10.1080/08120099.2019.1632224

Reid, A. J., & Payne, J. L. (2017). Magmatic zircon Lu–Hf isotopic record of juvenile addition and crustal reworking in the Gawler Craton, Australia. *Lithos, 292–293,* 294–306. https://doi.org/10.1016/j.lithos.2017.08.010

Reid, A. J., Zhao, Y., Wang, T., & Zhao, X. (2020). *Reconnaissance zircon U–Pb geochronology of the southeastern Olympic Cu–Au Province, South Australia.* Report Book 2020/00015. Department for Energy and Mining, South Australia, Adelaide.

Rubatto, D. (2002). Zircon trace element geochemistry: Partitioning with garnet and the link between U–Pb ages and metamorphism. *Chemical Geology, 184*(1–2), 123–138. https://doi.org/10.1016/S0009-2541(01)00355-2

Rudnick, R. L., & Gao, S. (2003). Composition of the continental crust. In R. L. Rudnick (Ed.), *The crust* (Vol. Treatise on Geochemistry, vol. 3, pp. 1–64). Elsevier/Pergamon.

Schaefer, B. F. (1998). *Insights into Proterozoic tectonics from the south-ern Eyre Peninsula, South Australia* [The University of Adelaide, PhD thesis (unpublished)]. Adelaide.

Schwarz, M. P. (2003). *LINCOLN, South Australia.* Primary Industries and Resources South Australia.

Shao, T., Xia, Y., Ding, X., Cai, Y., & Song, M. (2019). Zircon saturation in terrestrial basaltic melts and its geological implications. *Solid Earth Sciences, 4*(1), 27–42. https://doi.org/10.1016/j.sesci.2018.08.001

Skirrow, R. G., Bastrakov, E. N., Barovich, K., Fraser, G. L., Creaser, R. A., Fanning, C. M., Raymond, O. L., & Davidson, G. J. (2007). Timing of iron oxide Cu–Au–(U) hydrothermal activity and Nd isotope con-straints on metal sources in the Gawler Craton. *Economic Geology, 102*(8), 1441–1470. https://doi.org/10.2113/gsecongeo.102.8.1441

Skirrow, R. G., Wielen, S. E., Champion, D. C., Czarnota, K., & Thiel, S. (2018). Lithospheric architecture and mantle metasomatism linked to iron oxide Cu–Au ore formation: multidisciplinary evidence from the Olympic Dam Region. *Geochemistry, Geophysics, Geosystems, 19*(8), 2673–2705. https://doi.org/10.1029/2018GC007561

Sláma, J., Košler, J., Condon, D. J., Crowley, J. L., Axel, G., Hanchar, J. M., Horstwood, M. S. A., Morris, G. A., Nasdala, L., Norberg, N., Schaltegger, U., Schoene, B., Tubrett, M. N., & Whitehouse, M. J. (2008). Plešovice zircon—A new natural reference material for U–Pb

and Hf isotopic microanalysis. *Chemical Geology, 249*(1–2), 1–35. https://doi.org/10.1016/j.chemgeo.2007.11.005

Stacey, J. S., & Kramers, J. D. (1975). Approximation of terrestrial lead isotope evolution by a two-stage model. *Earth and Planetary Science Letters, 26*(2), 207–221. https://doi.org/10.1016/0012-821X(75)90088-6

Stern, R. A., Bodorkos, S., Kamo, S. L., Hickman, A. H., & Corfu, F. (2009). Measurement of SIMS instrumental mass fractionation of Pb isotopes during zircon dating. *Geostandards and Geoanalytical Research, 33*(2), 145–168. https://doi.org/10.1111/j.1751-908X.2009.00023.x

Stolz, A. J., Jochum, K. P., Spettel, B., & Hofmann, A. W. (1996). Fluid- and melt-related enrichment in the subarc mantle: Evidence from Nb/Ta variations in island-arc basalts. *Geology, 24*(7), 587–590. https://doi.org/10.1130/0091-7613(1996)024<0587:FAMREI>2.3.CO;2

Sun, S. S., & McDonough, W. F. (1989). Chemical and isotopic system-atics of oceanic basalts; implications for mantle composition and processes. In A. D. Saunders & M. J. Norry (Eds.), *Magmatism in the ocean basins* (pp. 313–345). Geological Society Special Publications 42. Geological Society London. https://doi.org/10.1144/GSL.SP.1989.042.01.19

Swain, G., Woodhouse, A., Hand, M., Barovich, K., Schwarz, M., & Fanning, C. M. (2005). Provenance and tectonic development of the late Archaean Gawler Craton, Australia; U–Pb zircon, geochemical and Sm–Nd isotopic implications. *Precambrian Research, 141*(3–4), 106–136. https://doi.org/10.1016/j.precamres.2005.08.004

Teng, X., & Santosh, M. (2015). A long-lived magma chamber in the Paleoproterozoic North China Craton: Evidence from the Damiao gabbro-anorthosite suite. *Precambrian Research, 256,* 79–101. https://doi.org/10.1016/j.precamres.2014.10.018

Tiddy, C. J., Betts, P. G., Neumann, M. R., Murphy, F. C., Stewart, J., Giles, D., Sawyer, M., Freeman, H., & Jourdan, F. (2020). Interpretation of a ca. 1600–1580 Ma metamorphic core complex in the northern Gawler Craton, Australia. *Gondwana Research, 85,* 263–290. https://doi.org/10.1016/j.gr.2020.04.008

Tiddy, C. J., & Giles, D. (2020). Suprasubduction zone model for metal endowment at 1.60–1.57 Ga in eastern Australia. *Ore Geology Reviews, 122,* 103483. https://doi.org/10.1016/j.oregeorev.2020.103483

Wade, B., Barovich, K., Hand, M., Scrimgeour, I. R., & Close, D. F. (2006). Evidence for early Mesoproterozoic arc-related magmatism in the Musgrave Block, central Australia: Implications for Proterozoic crustal growth and tectonic reconstructions of Australia. *The Journal of Geology, 114*(1), 43–63. https://doi.org/10.1086/498099

Wade, C. E., Payne, J. L., Barovich, K. M., & Reid, A. J. (2019). Heterogeneity of the sub-continental lithospheric mantle and 'non-juvenile' mantle additions to a Proterozoic silicic large igneous province. *Lithos, 340-341,* 87–107. https://doi.org/10.1016/j.lithos.2019.05.005

Watson, E. B., & Harrison, T. M. (1983). Zircon saturation revisited: tem-perature and composition effects in a variety of crustal magma types. *Earth and Planetary Science Letters, 64*(2), 295–304. https://doi.org/10.1016/0012-821X(83)90211-X

Williams, I. S. (1998). U–Th–Pb geochronology by ion microprobe. In M. A. McKibben, W. C. Shanks III, & W. I. Ridley (Eds.), *Applications of microanalytical techniques to understanding mineralizing processes* (Vol. 7, pp. 1–35). Reviews in Economic Geology.

Wingate, M. T. D., Campbell, I. H., Compston, W., & Gibson, G. M. (1998). Ion microprobe U–Pb ages for Neoproterozoic-basaltic mag-matism in south-central Australia and implications for the breakup of Rodinia. *Precambrian Research, 87*(3–4), 135–159. https://doi.org/10.1016/S0301-9268(97)00072-7

Zang, W. (2006). *MAITLAND Special, South Australia.* Primary Industries and Resources South Australia.

Zang, W., Fanning, C. M., Purvis, A. C., Raymond, O. L., & Both, R. A. (2007). Early Mesoproterozoic bimodal plutonism in the southeastern Gawler Craton, South Australia. *Australian Journal of Earth Sciences, 54*(5), 661–674. https://doi.org/10.1080/08120090701305210

Appendix 1.

Stratigraphic definition of Daly Head Metadolerite

Name: Daly Head Metadolerite

Derivation of name: Daly Head, a cape on KINGSCOTE 1:250 000 sheet, centred at 676100 mE, 6121950 mN, Z53

Distribution: Northern KINGSCOTE and southwestern MAITLAND 1:250 000 sheets. Recognised from coastal platforms Royston Head to Berry Bay.

Type locality: Royston Head.

Reference locality: Daly Head.

Age and evidence: Mesoproterozoic, SHRIMP U–Pb zircon age 1563 ± 4 Ma on metadolerite (gabbro) from Royston Head. Geochemical correlations with other straight-sided metadolerite dykes in the region.

Lithology: Metadolerite composed of hornblende–plagioclase–biotite ± clinopyroxene ± quartz. May have chilled margins and a weak alignment of hornblende and or biotite parallel to dyke margins. Clinopyroxene typically partly retrogressed to amphibole (cummintonite–grunerite).

Thickness: Straight-sided metadolerite dykes range from 5 m to <1 m thick.

Relationships and boundary criteria: Cross-cut deformation fabrics within the ca 1850 Ma Donington Suite. Some examples cut by narrow high-strain zones, within which a syn-kinematic granite has been dated to ca 1555 Ma.

Province: Gawler Craton

Parent: Nil

Synonymy: Previously referred as Tournefort Metadolerite by Zang (2006), and informally as 'Type 2 mafic dykes' by Reid et al. (2008).

Comments: Previous description of the Royston Head Granite precludes using Royston Head in the name of this unit, despite Royston Head being the type locality. Daly Head does contain similar metadolerite dykes that have been correlated based on geochemistry with the metadolerite dyke dated from Royston Head.